Journal of Materials Chemistry A

ROYAL SOCIETY OF CHEMISTRY

REVIEW

View Article Online
View Journal | View Issue

Cite this: J. Mater. Chem. A, 2024, 12, 6190

Recent progress in polyaniline-based chemiresistive flexible gas sensors: design, nanostructures, and composite materials

Jiayue Wen,[ab] Shang Wang, *[ab] Jiayun Feng,[a] Jingxuan Ma,[a] He Zhang,[a] Peng Wu,[a] Geng Li,[a] Zhuohuan Wu,[a] Fanzhou Meng,[a] Longqiu Li[ab] and Yanhong Tian *[ab]

Exposure to poisonous and hazardous gases such as NH_3, NO_2, and CO poses significant health risks. High-performance flexible gas sensors are essential for wearable real-time hazardous gas monitoring. Polyaniline (PANI) materials for gas sensing have advantages over conventional sensing materials like low working temperature, simple manufacturing, low cost, and high flexibility, which is particularly well suited for integrating into the developing Internet of Things to achieve real-time health monitoring or human–computer interaction. However, the PANI gas sensors still need to be improved with respect to their sensitivity, gas selectivity, or other aspects for practical applications. This article reviews three aspects including the PANI gas sensing mechanism, the nanostructure of PANI materials, and mixtures of PANI with other materials as flexible sensors. Nanostructures and nanomorphologies improved the sensor response due to the higher surface-to-volume ratio and abundant adsorption sites. Many innovative approaches to manufacturing composites allow the formation of heterojunctions at the interface to achieve better performance than chemiresistive PANI gas sensors. The synthesis protocols, structure engineering, underlying mechanisms, challenges, and future prospects of PANI sensors are also comprehensively reviewed.

Received 12th December 2023
Accepted 5th February 2024

DOI: 10.1039/d3ta07687c

rsc.li/materials-a

1. Introduction

With the rapid development of modern industry, large amounts of ammonia (NH_3), hydrogen sulfide (H_2S), nitrogen dioxide (NO_2), and other toxic gases are released into the environment surrounding us. According to the World Health Organization (WHO) database from April 2022, billions of people still breathe unhealthy air.[1] For example, NO_2 is associated with decreased lung function, increased respiratory symptoms, asthma, emergency room visits, hospital admissions, and premature deaths. NH_3 gas seriously endangers human health and can cause uremia, liver cirrhosis, kidney failure, and many other diseases.[2] Trimethylamine is an indicator for evaluating the degree of meat spoilage.[3] Humidity detectors, when integrated into functional

[a]State Key Laboratory of Advanced Welding and Joining, Harbin Institute of Technology, Harbin, 150001, China. E-mail: wangshang@hit.edu.cn; tianyh@hit.edu.cn; Tel: +86-451-86418359

[b]Zhengzhou Research Institute, Harbin Institute of Technology, Zhengzhou, 450000, China

Jiayue Wen

Jiayue Wen received his PhD degree from the Harbin Institute of Technology, Harbin, China in 2020. He is an associate professor at Zhengzhou Research Institute, Harbin Institute of Technology. His research interests are electronic packaging materials, flexible electronic devices, and gas sensors.

Shang Wang

Shang Wang received his PhD degree from the Harbin Institute of Technology, Harbin, China in 2019. He is currently working as an associate professor at the State Key Laboratory of Advanced Welding and Joining, Harbin Institute of Technology. His research interests are advanced packaging and reliability, printed electronics, and flexible electronics.

masks, offer significant potential for non-invasive disease diagnosis and wearable respiration monitoring.[4] However, harmful gases in low concentrations are often colorless and odorless and difficult to be felt by humans. Traditional gas sensors are also large or not portable. Consequently, developing flexible and wearable toxic gas sensors is of critical importance.

Since the first chemically reactive gas sensors were fabricated using tin dioxide and zinc oxide in the early 1960s, metal oxide semiconductor materials have been considered prime candidates for gas detection.[5] A variety of metal oxide gas sensors including tin oxide (SnO_2), zinc oxide (ZnO), cobalt oxide (Co_3O_4), tungsten oxide (WO_3), and iron oxide (Fe_2O_3) have been used in a variety of academic and commercial applications.[6,7] However, these sensors typically need to operate within a temperature range of 200–500 °C, which is not conducive to low-cost miniaturization of sensor devices and prevents sensors from being used in the emerging Internet of Things (IoT) applications such as e-skin.

In recent years, conductive polymer (CP) gas sensors have received increasing attention from researchers. Compared to metal oxide semiconductor materials, conductive polymers have been shown as room temperature highly sensitive materials for gas sensing. Besides, they have the advantages of low manufacturing process temperature, adaptable printing deposition processes, better flexibility, and low density, which makes conductive polymer materials promising for many emerging fields such as the Internet of Things, e-skin, and human–machine interaction. The most extensively studied conducting polymers are polyaniline (PANI), polypyrrole (PPy), polythiophenes (PTh), poly(3,4-ethylenedioxythiophene) (PEDOT), polyacetylene (PA) and their derivatives.[8–11]

PANI used as a gas-sensitive material in chemiresistive or heterostructure gas sensors, compared with other conductive polymer materials, presents the following advantages:[12–14] (a) simple and reversible doping–dedoping chemistry state in the presence/absence of the dopant molecule, (b) stable electrical conduction properties, (c) high environmental stability, and (d) the synthetic procedure is often easy and convenient. When doped PANI is exposed to reducing gases, such as NH_3, the resistance will increase. On the contrary, when undoped PANI is exposed to oxidizing gases, such as NO_2, the resistance will decrease. Obviously, an interfacial reaction occurs preferentially between gas and PANI. Therefore, morphology also plays an essential role in the gas sensing performance of PANI.

The disadvantages of the PANI material sensor are its poor environmental stability, and low selectivity and reproducibility. This is also a common problem for conductive polymer sensors. PANI can be combined with other materials (metals, metal oxides, carbon materials, MXenes, and MOFs) to improve 4S (sensitivity, speed, selectivity, and stability). In many research studies, better gas selectivity to detect NH_3, H_2, H_2S, CO_2, CO, NO_2, and volatile organic compounds (VOCs) has been demonstrated in PANI composites.

In this context, we review the recent progress in PANI-based gas sensors as shown in Fig. 1. Integrated manufacturing technology of flexible PANI gas sensing devices is introduced in detail. The gas sensing response mechanism of PANI and its composites is discussed first. Novel and familiar synthesis methods of different polymer structures (0D, 1D, 2D, and 3D) are summarized. The current state-of-the-art gas sensor material hybrids of PANI and inorganic materials are discussed.

2. Gas sensing mechanism

2.1. Gas sensing mechanism of PANI

A gas sensor can transform concentration signals of target gases into physical signals, including voltage, current or resistance outputs. When exposed to target gas analytes, the adsorption of gas molecules on PANI causes real-time resistance changes. Moreover, PANI exhibits excellent room-temperature gas sensing properties towards various gases.[15]

American Nobel laureate Mac Diannid proposed the most authoritative PANI molecular structure model. PANI chains consist of two structural units, a reduced [–B–NH–B–NH–] repeat unit and an oxidized [–B–N=Q=N–] repeat unit, in which B and Q respectively denote the C_6H_4 rings in the benzenoid and quinonoid forms, as shown in Fig. 2.[16,17] Different redox states can be converted to each other through specific redox reactions. Only the PANI in the intrinsic state can obtain conductive properties by doping, such as proton acid doping. As shown in Fig. 2a, the protonated PANI chain is electrically conductive only when $x = 0.5$ and $y = 0.5$, namely benzenoid : quinoid = 3 : 1. As shown in Fig. 2b and c, PANI has the ability of fast and reversible acid/base doping/dedoping. In acid or doped emeraldine salt form, PANI is conductive. Conversely, PANI is insulating in the dedoped form or emeraldine base form. After doping treatment, PANI will change from undoped insulating emeraldine base form to fully doped conducting emeraldine salt, and the conductivity will also increase from lower than 10^{-10} S cm^{-1} to higher than >1 S cm^{-1}, as shown in Fig. 2d.[18,19] After treatment with protonic acid or other oxidants, electrons in the PANI chain will be transferred to the oxidants, and the hole concentration in PANI will increase, forming p-type conduction.

p-Type conductive polymer materials have more stable chemical properties than n-type conductive polymer materials, which makes p-doping CPs more popular in academic research

Yanhong Tian

Yanhong Tian received her PhD degree from the Harbin Institute of Technology, Harbin, China in 2003. She is currently working as a professor at the School of Materials Science, Harbin Institute of Technology. She has been to the University of Waterloo, Canada, and the University of Maryland, USA as a post-doctor and visiting scholar. Her research interests include electronic packaging and materials science and flexible electronic materials and devices.

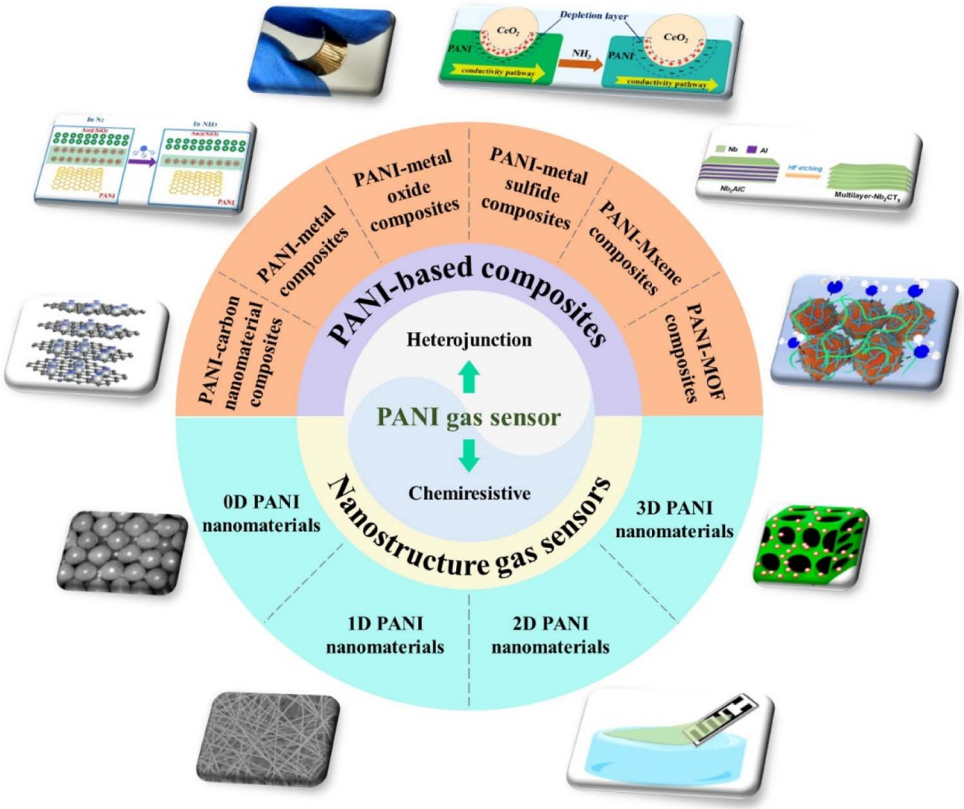

Fig. 1 An overview of the nanostructured PANI gas sensors and chemiresistive or heterojunction-based PANI composite gas sensors.

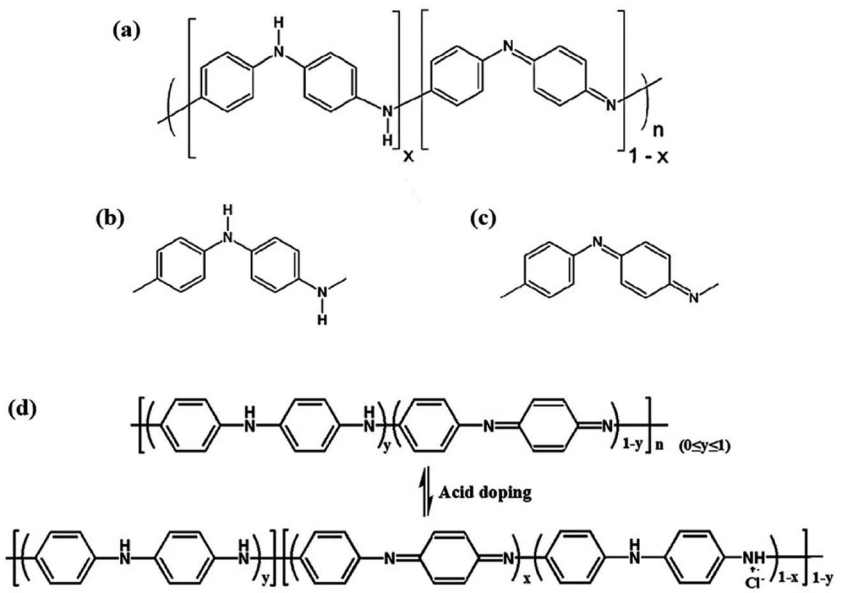

Fig. 2 A general chemical structure of polyaniline and its repeating units. (a) A general chemical structure of polyaniline, (b) reduced repeating unit, and (c) oxidized repeating unit. Reproduced from ref. 17 with permission from MDPI, copyright 2013. (d) Protonation/deprotonation process for the PANI sensing mechanism. Reproduced from ref. 18 with permission from Elsevier, copyright 2019.

and practical applications. PANI is also considered a p-type semiconductor material by default in this review.[9]

Many gases can change the redox state of PANI. When PANI is exposed to oxidizing gases such as NO_2, the NO_2 reacts with it to form the nitrogen dioxide anion (NO_2^-). The electrons in PANI are consumed, leading to an increase in hole concentration and a decrease in resistance. Acid gases such as HCl and H_2S can increase the proton concentration in PANI, which can

also reduce its resistance. In contrast, when reducing gases such as NH_3 interact with PANI, NH_3 molecules pull away and capture holes/protons from the amine group of PANI, which makes the sensor resistance increase significantly.[20,21]

2.2. Gas sensing mechanism of PANI composites

The combination of PANI and organic materials is mainly to improve the solubility and dispersion, and at the same time increase the contact area between the sensing material and the gas to be measured. However the gas sensing mechanism of PANI composites with inorganic materials is relatively more complex. In particular, there is a heterojunction between PANI and some semiconductor inorganic materials. Heterojunctions usually significantly enhance the gas sensing behavior of PANI composites. Fig. 3a and b show the energy band change after PANl comes in contact with the n-type inorganic material. At the contact interface, electrons diffuse from materials with high Fermi energy levels to materials with low Fermi energy levels. Eventually, the charge transfer creates a stable space charge region (depletion region) at the interface. The width of the depletion zone changes upon exposure to the target gas, resulting in a significant change in the resistance of the composites. Once exposed to oxidizing gas (such as NO_2), the NO_2 molecules would capture the electrons from the composite reducing the thickness of the depletion layer, as shown in Fig. 3c. In contrast, reducing gases (such as NH_3) would capture the protons from PANI, leading to an increase in the width of the interfacial depletion region, as shown in Fig. 3d.[9,22] This sensing mechanism is primarily used to explain the phenomenon of resistance changes in pure PANI materials when interacting with the target gas.

It is worth noting that the heterojunction can be either a p–n junction formed between p-type semiconductor PANI and an n-type semiconductor material or a Schottky junction formed by contacting p-type semiconductor PANI and a p-type semiconductor material. For example, a p–p junction can be formed between gallium nitride (GaN) (p-type semiconductor) and PANI (p-type conductive polymer) to achieve a gas sensing improvement effect, as shown in Fig. 4.[23] The interaction of NH_3 molecules with chemisorbed oxygen anions returns the trapped electrons to the surface of the gas sensing material, which will broaden the hole depletion layer. This mechanism is usually employed to explain the gas response when PANI forms a heterojunction with other semiconductors.

2.3. Computational research in PANI gas sensors

Computational studies have succeeded in elucidating the reaction mechanism, binding strength, charge transfer as well as other electronic and structural properties of the nanomaterials and the gas–sensor interaction. For PANI gas sensors, the most common computer research methods are density functional theory (DFT) and molecular dynamics (MD) simulations.

Density functional theory is a research method based on quantum mechanics. It can overcome the research blind spots in traditional characterization methods and can accurately

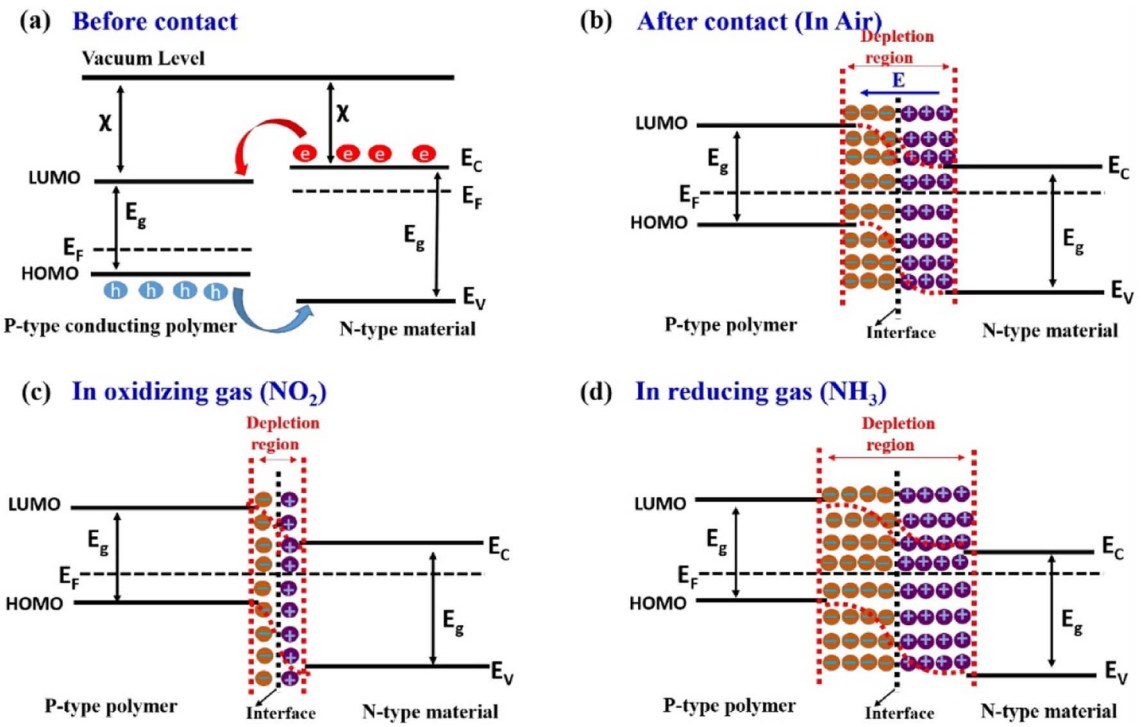

Fig. 3 Sensing mechanism of p-type conducting polymers and n-type inorganic material-based hybrid nanocomposites. Energy band diagram of the p-type conducting polymer and n-type material (a) before contact, (b) after contact in air, (c) after contact in oxidizing gas (NO_2) ambient, and (d) after contact in reducing gas (NH_3) ambient. Reproduced from ref. 22 with permission from Elsevier, copyright 2022.

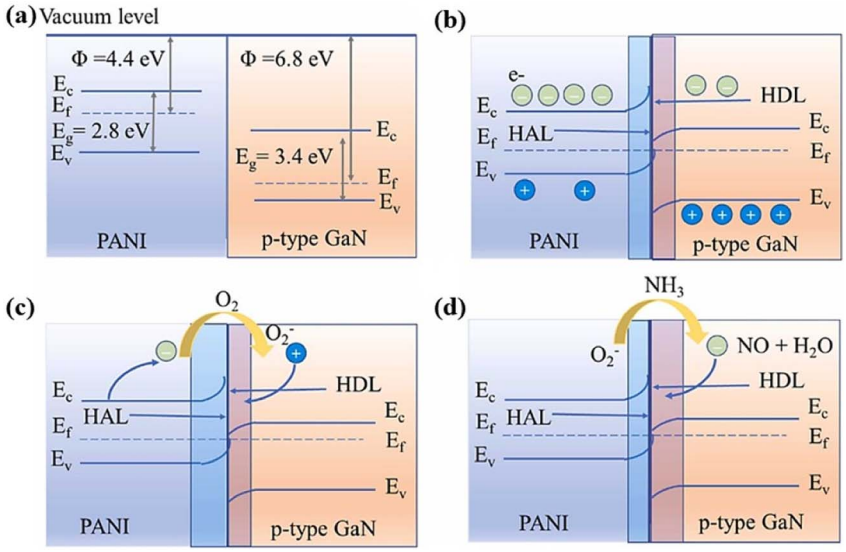

Fig. 4 (a) and (b) The energy band diagram of PANI and p-type GaN before and after contact, respectively. (c) and (d) The energy band structure of the PANI/p-type GaN heterojunction exposed to air and NH_3, respectively. Reproduced from ref. 23 with permission from Elsevier, copyright 2023.

obtain information such as the ground state energy, electronic structure, and geometric configuration of the atomic-scale gas–solid interface. DFT calculation is also a vital technique to reveal the gas–solid interface reaction mechanism and surface changes. For example, Amu-Darko *et al.*[24] used DFT calculations to investigate the electrical characteristics of In_2O_3/PANI composites. The research results show that the wave peak near the Fermi level has become significantly broader, and the 4d orbital of In has decreased, indicating that NO_2 has a better electrical adsorption effect on In_2O_3-PANI than O_2. The computational results also indicate that the NO_2 molecule adsorbs on the In atom surrounding PANI, reducing the distance between O–In from 3.128 Å to 2.35 Å, indicating the existence of adsorption between NO_2 gas and In_2O_3-PANI.

Unlike the ground-state calculations of DFT, first-principles molecular dynamics simulations do not ignore the kinetic energy of atoms. Thus, the influence of temperature on the system is included. Moreover, the time scale of its calculations is much longer, thus a dynamic process in a short period of time can be simulated. For instance, molecular dynamics simulations were performed to understand how ammonia molecules interact with HCl-doped PANI chains.[25] Molecular dynamics simulation results based on the PANI ammonia sensor show that ammonia molecules in the system prefer to be adsorbed by Cl^- rather than by H^+ or N^+ in the HCl-PANI chain, which facilitates the selection of precursor materials and the optimization of the synthesis process during the fabrication of next generation PANI sensors.

3. Nanostructures of PANI gas sensing materials

The nanostructure of PANI not only has an impact on sensing responses but is also crucial for the fabrication of flexible sensors. Improvements in sensing performance are mainly due to structural effects, such as adequate contact of the sensing material with the gas caused by the increase in specific surface area. Simultaneously, nanoparticles are suitable for manufacturing ink for flexible printed sensors to enhance consistency and stability. However, nanowires or two-dimensional PANI materials are very suitable for manufacturing flexible thin film sensors.

3.1. 0D PANI nanomaterials

Nanoparticles have a high specific surface area and can interact with gases in the environment to a greater extent, which is conducive to improving the sensitivity of gas sensing. The PANI nanoparticles are mostly synthesized by using micelles, emulsions, and inverse microemulsions and by dispersion polymerization. Individual PANI nanoparticle gas sensing materials mostly appeared in early research because it is generally believed that high-dimensional nanomaterials, such as nanowires or porous materials, have better sensing performance. Matsuguchi *et al.*[26] used polystyrene (PSt) microspheres as a template to prepare core–shell structure PSt@PANI(x) composite particles. The results show that the sensor response becomes better as the particle size increases. In essence, the three-dimensional space is constructed by PSt microspheres, which enhances the reaction between NH_3 molecules and PANI.

However, in a lot of studies on PANI nanoparticles, researchers find that PANI nanoparticles exhibit excellent dispersion and stability in solution. Im *et al.*[27] used DBSA as a surfactant and a dopant at the same time and prepared PANI nanoparticles with a diameter of 20–30 nm. The dispersion was left standing for more than one year without precipitation. This feature fits well with the performance requirements of the printable ink that has been developed rapidly in recent years. The PANI functional material is incorporated into the ink system and the printed electronics additive manufacturing

process, which could avoid repeated silicon-based deposition, lithography, and etching processes to fabricate light, thin, and flexible high-quality electronic sensors.[20,28] For example, Fisher *et al.*[29] realized the fabrication of PANI gas sensors based on the aerosol jet printing technology of additive manufacturing, which showed fast response characteristics in the required analysis range of 5–2000 ppm.

3.2. 1D PANI nanomaterials

One-dimensional PANI (1D PANI) gas sensing materials mainly include the preparation of linear PANI nanomaterials by chemical synthesis and the growth of PANI materials on one-dimensional nanowires or nanofiber templates. Bittencourt *et al.*[30] suggested that the one-dimensional PANI sensing material has a higher specific surface area, so the sensing performance is better.

The dispersive synthesis method is commonly used to quickly and efficiently synthesize large quantities of PANI nanofibers. By controlling the type and amount of surfactants, the shape and size of PANI nanofibers can be adjusted.[31] The synthesis process is usually carried out in the liquid phase, so it is very convenient for *in situ* protonic acid doping of PANI to adjust the gas sensing performance. As shown in Fig. 5a–c, Kulkarni *et al.*[32] used ammonium persulfate as an oxidant and hydrochloric acid as a dopant to prepare PANI nanofiber films. The diameters of prepared PANI nanofibers were 40–50 nm. The PANI nanofiber sensor demonstrated excellent selectivity with 11% response for 1 ppm concentration of NH_3. As shown in Fig. 5d–f, Kashyap *et al.*[33] synthesized PANI nanofibers by an *in situ* chemical oxidative polymerization method to detect toluene gas. The 1D PANI nanofibers had average diameters of 70–80 nm, and the length was calculated to be 400–450 nm. The better selectivity of the sensor had been observed since the CH_3 group of toluene was tightly conjugated to the NH group of the PANI nanofibers through non-covalent interactions.

Electrospinning is another common method to fabricate high-quality 1D PANI gas sensors. The electrospinning method can produce uniform thin films not only on flat surfaces but also on curved substrates. Compared with films manufactured by traditional processes, electrospinning fiber films have the advantages of more porosity, larger surface area, better flexibility, and better uniformity. However, due to the poor solubility of PANI and its brittleness, electrospinning of PANI is generally not performed directly. A common strategy is to use electrospinning fibers as templates on which PANI is polymerized to form fiber morphology, or 1D PANI fibers can also be fabricated using PANI blended with other polymers.[34,35] For example, PANI

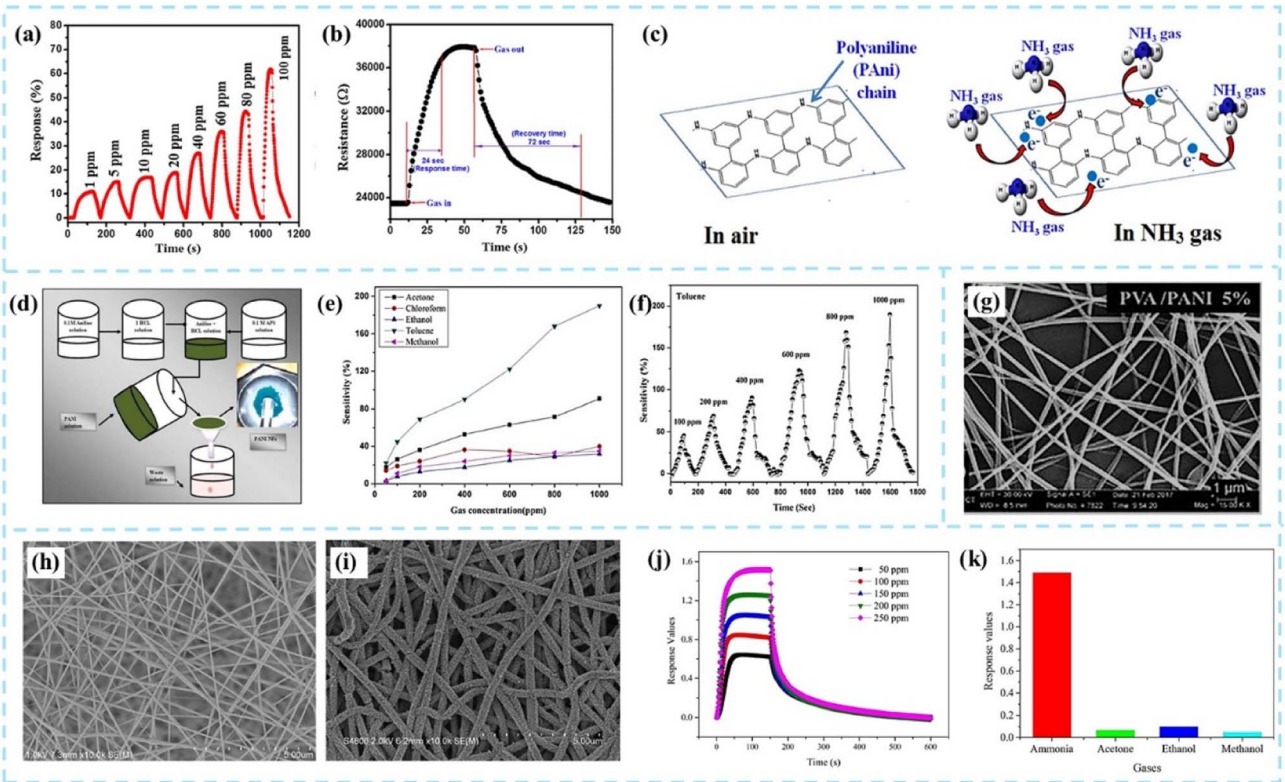

Fig. 5 (a and b) Dynamic response transients and the response/recovery time of the PANI nanofiber sensor. (c) Schematic of the gas sensing mechanism of the PANI nanofiber sensor for NH_3. Reproduced from ref. 32 with permission from Springer Nature, copyright 2019. (d) Synthesis procedure of PANI NFs. (e and f) Sensitivity of the PANI sensor as a function of VOC gas concentration and dynamic sensitivity of the PANI sensor for toluene. Reproduced from ref. 33 with permission from IOP Publishing, copyright 2014. (g) SEM images of the PVA/PANI homogeneous fibers. Reproduced from ref. 30 with permission from John Wiley and Sons, copyright 2018. SEM images of (h) PA6 and (i) PA6/PANI nanofibers. (j) Dynamic response of the sensor for ammonia concentrations from 50 to 250 ppm. (k) Selectivity of PA6/PANI nanofiber sensors. Reproduced from ref. 25 with permission from American Chemical Society, copyright 2021.

and poly(vinyl alcohol) (PVA) can be co-electrospun together (Fig. 5g).[30] The process conditions such as the ratio between PANI and the polymer, electrostatic spinning voltage, liquid flow rate, and ambient temperature during the spinning process not only affect the fiber morphology but also directly impact the response performance of the sensors.

Pang *et al.*[25] prepared polyamide 6 (PA6)/PANI nanofibers using electrospun PA6 nanofibers as a template, as shown in Fig. 5h–k. The PA6/PANI nanofiber was fabricated by *in situ* polymerization of aniline and hydrochloric acid (HCl) as a dopant for PANI. Sensors showed stable dynamic response curves with the increase of ammonia concentration from 50 ppm to 250 ppm. Sonwane *et al.*[36] used a solution of polyvinylpyrrolidone (PVP) and the $NiFe_2O_4$ precursor to fabricate electrospun nanofibers. The collected nanofibers were calcined at 600 °C for 2 hours to prepare ferrite $NiFe_2O_4$ fibers. $NiFe_2O_4$/PANI composite nanofibers were synthesized by *in situ* polymerization of the aniline monomer in the presence of as-synthesized $NiFe_2O_4$ nanofibers. Compared with PANI, the *in situ* polymerized $NiFe_2O_4$/PANI composite nanofibers exhibited higher sensitivity to ammonia at room temperature. The improvement in sensing performance is primarily attributed to the fact that $NiFe_2O_4$ is an n-type semiconductor nanomaterial that can form a p–n junction with p-type PANI, resulting in a response value that is nearly three times higher than that of the original PANI. Sensors showed a maximum sensing response of 30.8 with a fast response/recovery time (15 s/21 s) for 100 ppm of ammonia.

In addition, many fabrics are made of fibers and can serve as two-dimensional templates for sensors. Kim *et al.*[37] utilized the filtering layer of a mask, made of polypropylene fibers (PP fibers), as a flexible substrate to create PANI/$Ti_3C_2T_x$ functionalized mask sensors. These sensors are primarily designed to monitor carbon dioxide and human respiration rates. The resulting gas sensors exhibit a wide detection range (25–1500 ppm), reliable reproducibility, long-term stability, and excellent flexibility and selectivity. Their response to 500 ppm CO_2 was remarkable (15.2%), which is 6.5 times higher than that of traditional $Ti_3C_2T_x$ gas sensors and 2.4 times higher than that of the original PANI.

3.3. 2D PANI nanomaterials

Two-dimensional PANI (2D PANI) nanostructures are the focus of research for chemiresistive gas sensors due to their unique 2D geometry, nanoscale thickness, and ultra-high surface area. The two-dimensional PANI nanomaterials, including nanosheets, nanofilms, nanoplates, *etc.*, have a thickness ranging from a few nanometers to tens of nanometers, and their lateral dimensions can reach several centimeters.

Electrochemical deposition is an effective method for preparing 2D PANI thin films on conductive substrates. The deposition process affects the morphology of PANI and the thickness of the film, which in turn affects the gas sensing performance. Korent *et al.*[38] directly electrochemically deposited PANI films on commercial gold screen-printed electrodes without using complex dopants and nanomaterials other than hydrochloric acid as a dopant. As shown in Fig. 6a, the sensor showed a limit of detection of 23 ppb and good sensitivities with 12.30% for 32–200 ppb and 4.27% for 200–1000 ppb, respectively. Popov *et al.*[39] prepared PANI, PEDOT, and PANI-PEDOT composite films through electrochemical deposition on the surface of the ITO substrate. In this study, the conductivity and sensitivity of the deposited film increased when synthesizing PANI in the presence of 3,4-ethylenedioxythiophene (EDOT). The response time of the PANI-PEDOT film was 6 times faster than that of PANI films deposited under similar electrochemical polymerization conditions.

Spin coating is another common method for preparing soluble polymer films, but PANI cannot be dissolved in most organic solvents. Although PANI can be dissolved in a small amount in strong polar solvents such as dimethylformamide (DMF), it is not enough to prepare uniform PANI films by the spin coating method. However, through the chemical copolymerization method, the solubility and operability of PANI can be effectively improved, and more functionality can be given to it. Copolymerization methods are usually graft or block. Ali *et al.*[40] incorporated PANI in a poly(methyl methacrylate) (PMMA)/polystyrene (PS)/multi-walled carbon nanotube (MWCNT) blended matrix and optimized the electrical properties as well. In addition to realizing the conventional NH_3 gas sensing function, the MWCNTs/PMMA in the sensor material jointly improved the hydrophobicity of the material, enabling PANI to exhibit a more excellent gas response at higher humidity. Shaari *et al.*[41] reviewed the preparation methods and performance studies of PANI and the PMMA copolymer and blended composites. After copolymerization or blending, the solubility and mechanical properties of PANI composite materials are significantly improved. However, the crystallinity of the copolymer will decrease with the polymerization process, which will have a negative impact on the electrical conductivity, sensing properties, and photoelectric properties of the material. Therefore, much work remains to be done for the optimization of the above physical property.

Layer-by-layer (LBL) self-assembly is a simple and versatile surface modification method in which the substrate is alternately immersed in a polyanionic and polycationic solution to prepare alternating composite films consisting of two polyelectrolytes.[42] Graboski *et al.*[43] used a spin-assisted layer-by-layer assembly method to create PANI-based multilayer films, which resulted in significantly improved chemical and electrochemical stability compared to the PANI homopolymer. In this study, the LBL PANI multilayer film presented the highest roughness value, as shown in Fig. 6b. The LBL sensors exhibited better response values and realized the distinction of 3 different artificial aromas (apple, strawberry, and grape). Zhu *et al.*[44] prepared PANI films functionalized with different surfactants (SDBS, SDS, and LA) by the interface synthesis method, as shown in Fig. 6c. The addition of surfactants made the structure of the film more regular, improved the crystallinity of the film, accelerated the movement of electrons in the PANI chain, and improved the sensitivity and detection limit. In the research by Zhang *et al.*,[45] the surfactant monolayer was the key factor for

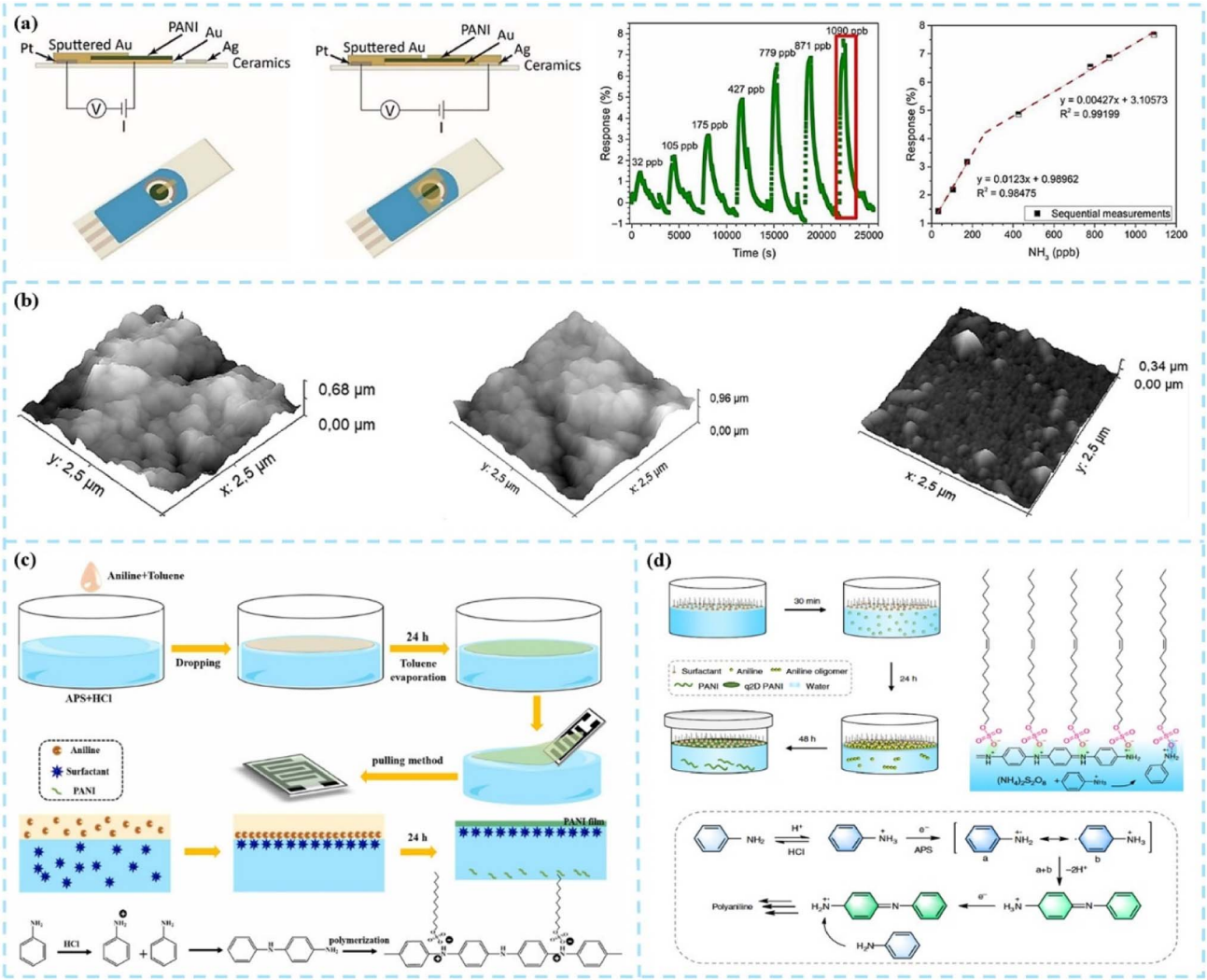

Fig. 6 (a) Scheme of preparing PANI-Au-SPE samples and PANI-Au-SPE sensor's response after exposing to different concentrations of gas. Reproduced from ref. 38 with permission from MDPI, copyright 2021. (b) AFM 3D images of the gas sensors coated with PANI-*in situ*, PANI interfacial/PSS LbL, and PANI-*in situ*/PSS LbL films. Reproduced from ref. 43 with permission from Elsevier, copyright 2018. (c) Synthetic schematic diagram of PANI films and the mechanism of polymerization of aniline. Reproduced from ref. 44 with permission from Elsevier, copyright 2022. (d) Synthetic procedure of q2D PANI and the reaction mechanism. Reproduced from ref. 45 with permission from Nature, copyright 2019.

the morphologies of 2D PANI. The synthesis procedure is schematically illustrated in Fig. 6d.

3.4. 3D PANI nanomaterials

Three-dimensional PANI (3D PANI) materials have an interconnected three-dimensional network and a highly continuous porous structure. Compared with 1D or 2D materials, the interface reactions between gas molecules and 3D PANI nanostructures are more abundant, which is beneficial to improve the sensitivity of gas sensors. Here we present several common methods for the preparation of 3D PANI nanostructures.

Chemical polymerization is often used for the synthesis of PANI nanoparticles or nanowires because some surfactants can form micelles in a liquid environment after dissolution. Using this soft template method, the aniline polymerization process will spontaneously generate a three-dimensional nanostructure.

Most inorganic nanomaterials have a crystal structure. Compared with organic materials, it is easier to prepare three-dimensional nanocomposites. The inorganic 3D materials can be used as a template to synthesize 3D PANI materials with richer morphology, and the p–n junction between inorganic materials and PANI will further improve the sensing performance. Wang *et al.*[46] used quasi-graphite capsules (GCs) as templates to synthesize an ultrathin 3D hollow GCs/PANI hybrid composite by *in situ* polymerization. GCs had a capsule-like hollow/open structure providing a large surface area for ammonia adsorption and enhancing the structural stability of hybrids. Due to the large interfacial surface area of GCs/PANI, it was highly sensitive to 10 ppm NH_3 gas with a response and recovery time of 34 s and 42 s, respectively. Wang *et al.*[47] synthesized α-Fe_2O_3 nanotubes by an anion-assisted hydrothermal route, which has a smooth surface and three-dimensional hollow structure. PANI was

uniformly coated on the surface of α-Fe_2O_3 by *in situ* chemical oxidation polymerization. Li *et al.*[48] synthesized flower-like WO_3 materials as three-dimensional templates by a hydrothermal method. The PANI@flower-like WO_3 nanocomposite was also synthesized by a facile chemical oxidation polymerization method. The excellent NH_3 sensing properties with a detection limit of 0.5 ppm were attributed to its unique 3D structure and the p–n heterojunction formed at the interface between PANI and flower-like WO_3.

In situ chemical or electrochemical polymerization on organic 3D substrates can also be used to prepare 3D structured PANI. As shown in Fig. 7a, Yang *et al.*[49] *in situ* oxidatively polymerized PANI on bacterial cellulose (BC) 3D network substrates. The composite material sensor not only had a high specific surface area and 3D network but also co-doped sulfosalicylic acid (SSA) and poly(2-acrylamido-2-methyl-1-propane sulfonic acid) (PAMPS). SSA served as the doping sites to prolong the conjugation length of PANI to promote intrachain charge transport. PAMPS provided numerous sulfonic acid groups resulting in the increase of interchain conductivity. With the above synergistic effect, the bacterial cellulose/polyaniline ammonia sensor achieves a fast response/recovery time of 4.1 s/16 s for 50 ppm ammonia and

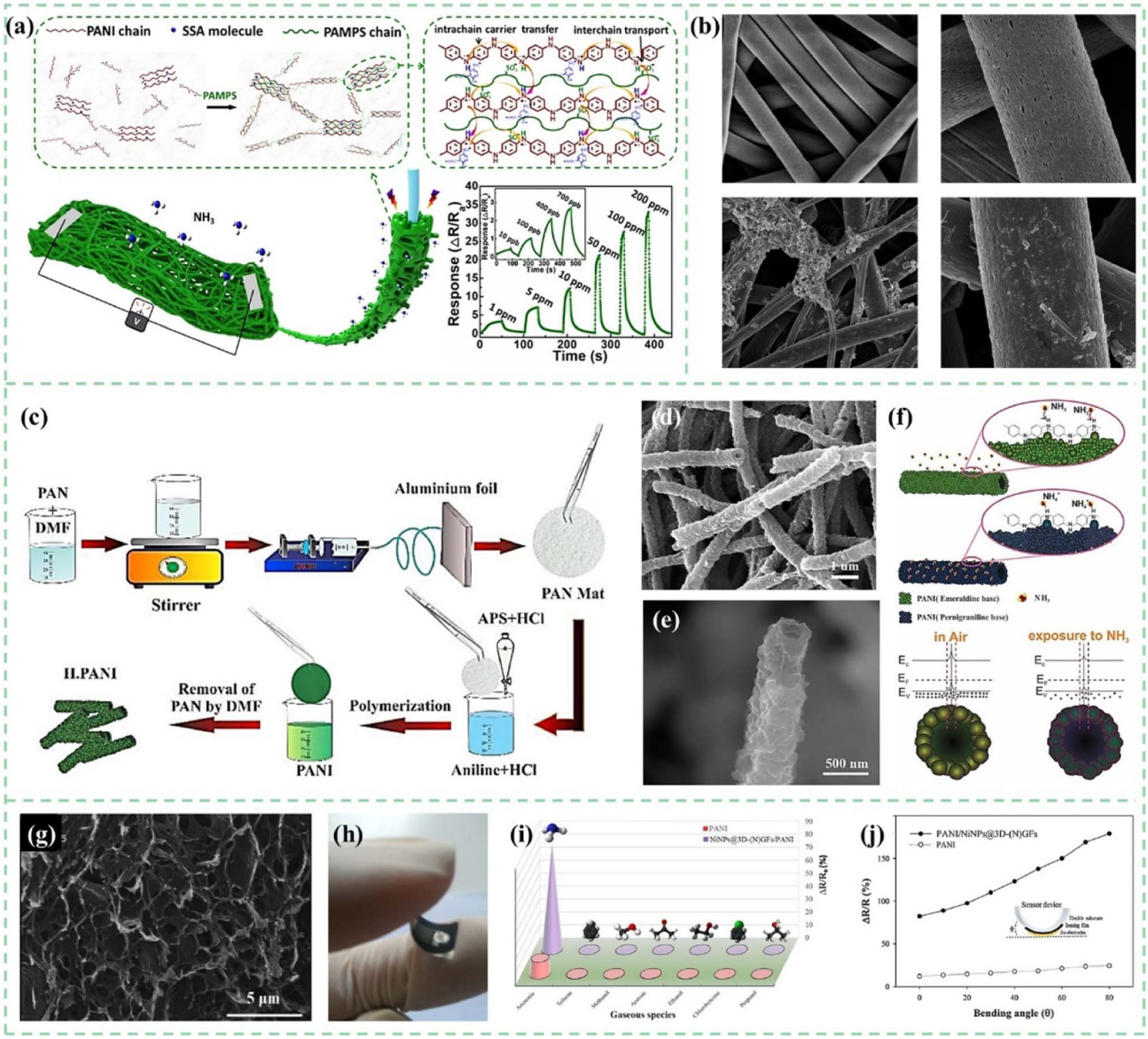

Fig. 7 (a) Schematic demonstration of the BC/PANI-SSA/PAMPS composite, with enlarged boxes showing the interactions of BC and PANI, and the schematic presentation of the proposed working method of co-doping PANI. Reproduced from ref. 49 with permission from Elsevier, copyright 2021. (b) SEM images of electrospun PS fibers and PANI-coated PS fibers. Reproduced from ref. 50 with permission from the Royal Society of Chemistry, copyright 2019. (c) Fabrication procedure of the core/shell hollow polyaniline sensor. (d and e) SEM images of the hollow nanofiber structure of polyaniline. (f) Conversion of emeraldine salt to pernigraniline base upon exposure to NH_3 and the energy band diagram of PANI before and after exposure to ammonia gas. Reproduced from ref. 51 with permission from IEEE, copyright 2019. (g) SEM images of 3D-(N) GFs. (h) Schematic diagram of flexible gas sensors. (i and j) Selectivity and flexibility of the pure PANI and Ni NPs@3D-(N)GFs/PANI hybrid gas sensors upon exposure to 100 ppm NH_3. Reproduced from ref. 52 with permission from Elsevier, copyright 2019.

a low detection limit of up to 10 ppb. In another study, plasma-treated functionalized electrospun polystyrene (PS) nanofibers were used as templates to fabricate 3D structured PANI sensors. As shown in Fig. 7b, PANI and graphene-PANI were coated on a PS membrane using an *in situ* chemical polymerization casting method by Bhadra *et al.*[50] It was observed that the thermal stability of the nanocomposite sensor material was significantly enhanced. The flexible membranes coated with polyaniline–graphene/polystyrene nanocomposites could be used to fabricate high-performance CO_2 gas sensors with fast response time and recovery time of both 65 s.

The principle of the sacrificial template method is similar to the above process, using a solvent to dissolve or corrode the 3D template, leaving only the 3D PANI gas sensing material. PS, SiO_2, polymer nanofibers, and many other materials can be used as templates. As shown in Fig. 7c–f, Safe *et al.*[51] used electrospun polyacrylonitrile (PAN) as a hard template. The PANI material was polymerized *in situ* on the surface of PAN fibers. Core/shell nanofibers were washed with DMF to remove the PAN core. Compared to PANI powder sensors, the nanotubular structured PANI sensor with a higher surface area to volume ratio and high porosity allowed the sensor to reach a detection limit of 81 ppb for ammonia gas.

The freeze-drying method is a common manufacturing process of aerogels. Aerogels are light in mass and have a rich porous structure inside. Combined with the oxidation polymerization process, the preparation of a three-dimensional structure PANI aerogel can be realized conveniently. Tabr *et al.*[52] used a freeze-drying method to prepare a 3D nitrogen-doped graphene-based framework on which nickel nanoparticles were decorated, and PANI was synthesized by *in situ* oxidative polymerization on a flexible thin substrate, as shown in Fig. 7g–j. Synergetic behavior between both components manifested outstanding sensitivity with 750.2 at 1000 ppm NH_3. Tohidi *et al.*[53] prepared reduced graphene oxide (rGO)/PANI hybrid hydrogels and used a freeze-drying method to prepare 3D networks. In this study, the effect of the ratio of graphene and PANI on the sensing performance was compared. The response of the 3D rGO/PANI (1 : 1) hybrid sensor reached 17.4% for 100 ppm NH_3, which was 44.7 times higher than that of a 3D rGO sensor.

4. PANI-based composite gas sensing materials

In addition to improving the performance of PANI gas sensors based on their morphology and structure, the composition of PANI-based materials will also have a significant impact on the sensitivity, selectivity, and stability of the sensor. Here we review recent progress in the composites of PANI and carbon nanomaterials/metals/metal oxides/metal sulfides/MXenes/MOFs and analyze the role of composite materials in providing active sites, increasing carrier concentration, and constructing heterojunctions. A summary of the gas sensing performance of different PANI-based composites is presented in Table 1.

4.1. PANI-carbon nanomaterial composites

Carbon nanomaterials have excellent physical and chemical properties. For example, reduced graphene oxide has more gas adsorption sites due to the oxygen functional groups attached to graphene nanosheets.[98–101] One-dimensional carbon fibers can be easily combined with cotton fabrics to develop flexible and wearable gas-sensing devices.[102,103] Multi-walled carbon nanotubes have high electrical conductivity and excellent mechanical properties. To create high-efficiency gas sensors, research on carbon nanomaterials and PANI composites has attracted much attention.

Umar *et al.*[104] synthesized PANI/Ag_2O/GO composites with a mixing method followed by an ultrasonication process, as shown in Fig. 8a and b. The composites were then utilized as a chemiresistive sensor for NO_2 gas detection. Compared to the pure PANI and PANI/Ag_2O composites, the incorporation of GO enhanced sensitivity from 2.5 and 3.25 to 5.85 for 25 ppm target gas concentration. In many other studies, composites of rGO and PANI have been confirmed to have better sensing performance as well. Luo *et al.*[105] successfully used an *in situ* polymerization technique to coat these composites on cotton threads to construct room-temperature NH_3 sensors. The sensing mechanism of the composite material is believed to be the p–p heterojunction between PANI and rGO, and PANI and rGO formed π–π conjugates, which is beneficial for the rapid transport of carriers. Compared to the pristine rGO and PANI, the response sensitivity of hybrid sensors with a heterostructure increased by 4–5 times. As shown in Fig. 8c and d, Zhang *et al.*[106] synthesized tin oxide/reduced graphene oxide/polyaniline (SnO_2/rGO/PANI) through *in situ* polymerization for a sub-ppb H_2S gas sensor at room temperature.

The three-dimensional structure of SnO_2 hollow spheres and the large specific surface area of graphene significantly enhance the PANI sensor's performance. Two different types of heterojunctions, at the surface of oxygen species adsorbed on the SnO_2 and interface of the SnO_2 and the PANI, respectively, lead to better sensitivity. Moreover, p–n junctions formed by the rGO and SnO_2 hybrid interface further improved the sensing properties, so the sensing composites achieved a detection limit of 50 ppb. As shown in Fig. 8e, SnO_2/rGO/PANI flexible sensors showed good stability and flexing resistance after 60 bending cycles. Singh *et al.*[107] reported a PANI/montmorillonite (MMT)-rGO nanocomposite that exhibited excellent sensing response to HCN gas detection. The addition of rGO significantly enhanced the sensitivity of the PANI/MMT material to HCN gas, increasing it from 0.89 ppm^{-1} to 1.1174 ppm^{-1}. Due to the advantages of high specific surface area, porous structure, and high adsorption coefficient of MMT, the sensor automatically recovered within 25 seconds.

Carbon nanotubes not only have excellent mechanical, electrical, chemical, and low-temperature operational characteristics, but they also have a large surface area and exhibit high sensitivity to gases such as SO_2, NO, NO_2, NH_3, H_2, and others.[108] An interconnected mesoporous network structure will be formed in the composite material of carbon nanotubes and PANI. This also affects the conductivity characteristics of PANI/CNTs composite materials, improving the transport rate of

Table 1 Comparison of the gas sensing response of different PANI-based composite gas sensors

Materials	Structures	Gas	Sensing range (ppm)	Sensitivity or response	Response time/recovery time (s)	Reference
PANI/rGO	Nanosheets	NH_3	0.3–15	13% (15 ppm)	96/1326	2
PANI/rGO	Nanosheets	NH_3	0.046–50	15% (5 ppm)	75/—	54
PANI/nitrogen-doped graphene quantum dots/In_2O_3	Nanofiber	NH_3	0.6–2	15.2% (1 ppm)	—	55
PANI/CNTs	Fiber	NH_3	0.5–70	452% (70 ppm)	93/36	56
PANI/CNTs	Fiber	NO_2	10–50	65.9 (50 ppm)	5.2/3.2	57
PANI/MWCNTs	Film	NH_3	0.01–40 ppm	11.8 (40 ppm)	—/236	58
PANI/MWCNTs	Film	H_2	0.4%	24% (4000 ppm)	48/55	59
PANI/MWCNTs	Fiber	NH_3	0.2–100	92% (100 ppm)	9/30	60
PANI/MWCNTs	Film	NH_3	4–1000	40% (30 ppm)	18/46	61
PANI/MWCNTs	Film	NH_3	5–1000	429% (25 ppm)	213/98	62
PANI/activated charcoal	Nanoparticles	Methanol	50–200	43% (200 ppm)	25/305	63
PANI/hollow C/In_2O_3	Nanofiber	NH_3	0.6–2	18.2 (1 ppm)	—	64
PANI/TiO_2/Au	Film	NH_3	1–50	123% (50 ppm)	52/122	65
PANI/SnO_2	Nanocomposite	NH_3	0.01–100	29.8 (100 ppm)	125/167	18
PANI/SnO_2	Nanotube	NH_3	20–100	35.4 (100 ppm)	—	66
PANI/SnO_2	Film	H_2	6000	42% (6000 ppm)	11/7	67
PANI/Cu-doped SnO_2	Web-like nanofibers	NH_3	0.01–100	25.3 (50 ppm)	52/121	68
PANI/Ni@ZnO	Film	NO_2	5–100	75% (100 ppm)	82/399	69
PANI/ZnO	Film	NO_2	20	611 (20 ppm)	130/210	70
PANI/Ag-decorated ZnO	Nanorods	NH_3	5–120	50% (50 ppm)	23/58	71
PANI/Ce/ZnO	Nanoparticles	Liquefied petroleum gas	30–330	80% (100 ppm)	157/154	72
PANI/ZnO	Hollow sphere	NH_3	0.5–100	6 (10 ppm)	140/136	73
PANI/Fe_2O_3	Film	NO_2	20	229 (20 ppm)	141/228	74
PANI/Fe_2O_3	Nanosheet	NH_3	0.5–10.7	54% (0.5 ppm)	—	75
PANI/GO/PANI/ZnO	Film	NH_3	25–500	38.31% (100 ppm)	30/—	76
PANI/$CuFe_2O_4$	Nanocomposite	NH_3	1–50	27.37% (5 ppm)	84/54	77
PANI/WO_3	Hollow sphere	NH_3	0.5–100	6.25 (10 ppm)	136/130	78
PANI/WO_3	Film	NO_2	2–30	60.19 (30 ppm)	—	79
PANI/WO_3	Nanocomposite	H_2	1–100	2.62% (5 ppm)	200/225	80
PANI/CeO_2	Nanohybrid	NH_3	10–100	93% (100 ppm)	8/482	81
PANI/TiO_2	Nanocomposite	NH_3	0.5–100	5.4 (100 ppm)	100/232	82
PANI/In_2O_3	Nanosheet	NO_2	0.3–100	12.8 (3 ppm)	17.28/91.26	24
PANI/V_2O_5/Pb_3O_4	Powder	CO	100–2 25 000	23.82% (100 ppm)	34/37	83
PANI/CuO	Nanoparticle	H_2S	2–25	25% (8 ppm)	36/71	84
PANI/MoS_2	Nanosheet	NH_3	0.5–2	—	14/16	85
PANI/MoS_2/Pt	Nanocomposite	NH_3	0.25–500	16.64 (50 ppm)	15/103	86
PANI/WS_2	Fiber	NH_3	50–200	81% (200 ppm)	260/790	87
PANI/black phosphorus	Two-dimensional material	NH_3	1–4000	About 2.5 (50 ppm)	28/46	88
PANI/$Ti_3C_2T_x$	MXene composites	Ethanol	50–200	41.4% (200 ppm)	0.4/0.5	89
PANI/$Ti_3C_2T_x$	Nanofibers	NH_3	5–100	55.9% (20 ppm)	—	90
PANI/V_2C	MXene composites	NH_3	0.3–10	27% (5 ppm)	3/8	91
PANI/g-C_3N_4	Nanocomposites	NH_3	0.5–200	19.5 (200 ppm)	134/624	92
PANI/g-C_3N_4	Nanosheet	NO_2	8–108	92% (108 ppm)	—	93
PANI/SnO_2/Zn_2SnO_4	Porous nanosphere	NH_3	0.5–100	20.4 (100 ppm)	46/54	94
PANI/$NiCo_2O_4$	Nanorod	NH_3	0.5–20	4.67 (20 ppm)	25/59	95
PANI/$NiCo_2O_4$	Nanofibers	NH_3	1–500	337 (100 ppm)	55/80	96
PANI/PEO	Fiber	H_2S	1–10	5% (1 ppm)	120/250	97

charge carriers and increasing the number of active sites, ultimately enhancing gas sensing performance. Roy *et al.*[109] synthesized PANI-MWCNT composites through *in situ* polymerization for rapid detection of CO at room temperature. The PANI-MWCNTs exhibit a higher response for 500 ppm CO among the test gases towards saturated 2-propanol, acetone, ethanol, methanol, ammonia, *etc.* In particular, the selectivity of the sensor to CO is better than that of ammonia.

As shown in Fig. 8f–h, Ma *et al.*[110] used ethylenediamine (EDA) for the surface treatment of PET fibers and then put them into MWCNT dispersion. The carboxyl groups (–COOH) on the surface of MWCNTs will adsorb to the exposed amino groups (–NH_2) on the surface of PET. The electrons quickly transport from PANI to MWCNTs. Gas sensing properties for ammonia and adhesion performance between the sensing materials and flexible substrates have been improved simultaneously.

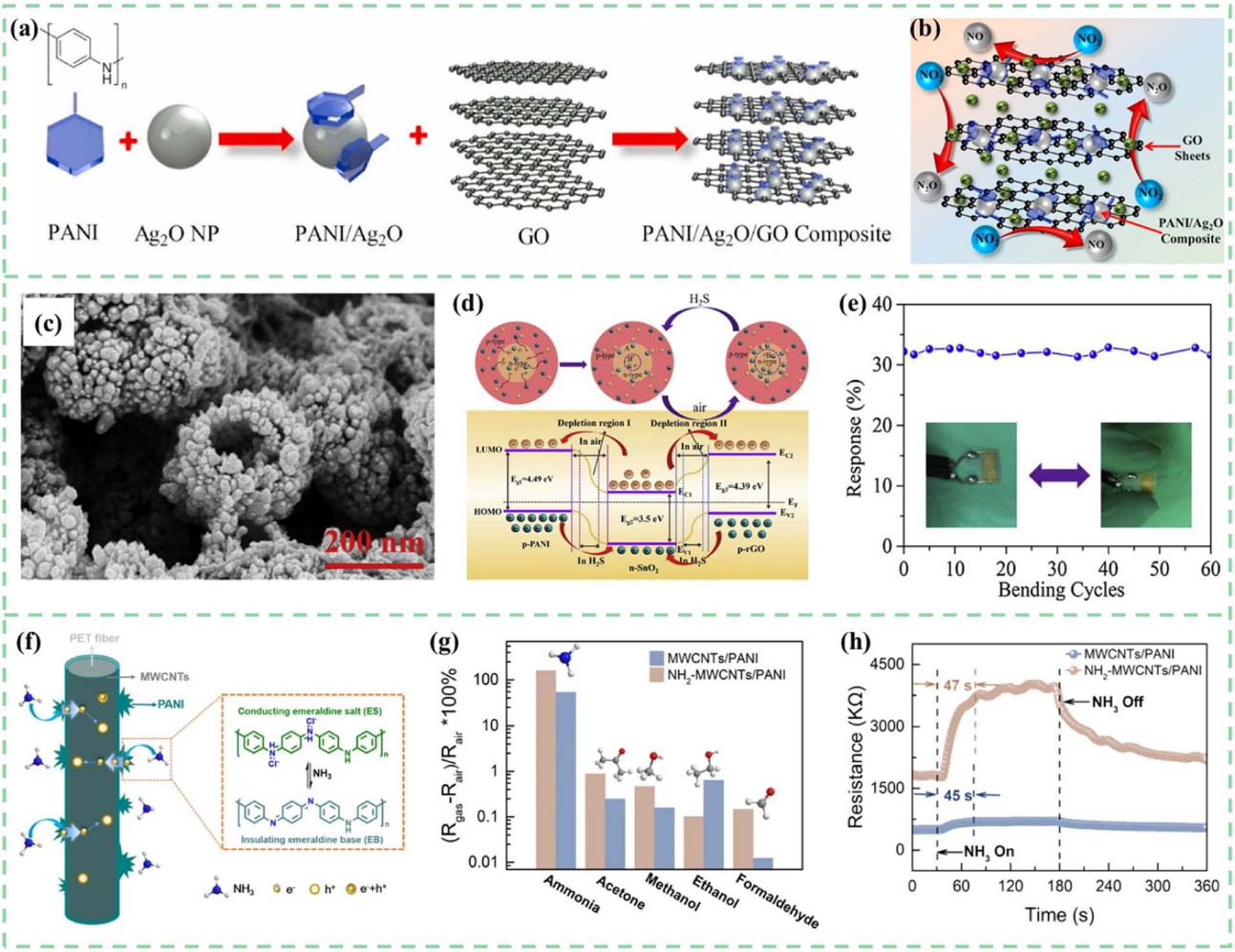

Fig. 8 (a) Schematic for the synthesis of PANI, Ag_2O nanoparticles, PANI/Ag_2O nanoparticles, and PANI/Ag_2O/GO composites. (b) Proposed gas sensing mechanism of the fabricated PANI/Ag_2O/GO nanocomposite-based NO_2 gas sensor. Reproduced from ref. 104 with permission from Elsevier, copyright 2021. (c) SEM images of *in situ* polymerized SnO_2/rGO/PANI samples. (d) Mechanism diagram of the SnO_2/rGO/PANI nanocomposite toward H_2S gas. (e) Response of the flexible sensor towards 500 ppb H_2S after some bending cycles. Reproduced from ref. 106 with permission from Elsevier, copyright 2019. (f) The NH_3 sensing mechanism of PET-NH_2-MWCNTs/PANI. (g) The response to various gases, and (h) the response time to 50 ppm NH_3 for PET-MWCNTs/PANI and PET-NH_2-MWCNTs/PANI sensors. Reproduced from ref. 110 with permission from Elsevier, copyright 2021.

4.2. PANI-metal composites

Many metal nanoparticles (MNPs) have been combined with PANI to improve gas-sensing properties. For example, Ag, Au, Pd, Pt, Cu, Ni, and many other metal nanomaterials have been reported. These hybrid nanocomposites incorporate the advantages of both the metal nanoparticles and PANI.

Metal nanoparticles typically exhibit high electrical conductivity. The combination of metal nanoparticles with PANI can directly modify the electrical properties of the composite material, thereby enhancing its gas response sensitivity. Metal nanoparticle modification can accelerate the charge transfer between PANI and gas molecules, further improving the sensing performance and stability. In addition, because certain metals exhibit better absorption characteristics for a specific gas, their combination with PANI can enhance the selectivity of gas sensors.[111]

Ag nanoparticles have high conductivity and excellent stability. Adhav *et al.*[112] synthesized PANI-Ag nanocomposites by an *in situ* oxidative polymerization method using ammonium persulphate as an oxidizing agent. In this process, Ag nanoparticles synthesized using an ultrasonic processor were added. The presence of Ag nanoparticles improved the conductivity of the formed PANI-Ag nanocomposite and shortened the response time of the developed sensor. The sensor showed a quick response and recovery time (30 s/120 s) towards ammonia at 1–100 ppm concentration.

Nasresfahani *et al.*[113] synthesized Au/PANI nanocomposites by the ultrasound mixing of emeraldine salt PANI and different amounts of Au nanoparticles colloidal solution. When the Au NPs were introduced into PANI, these NPs were thought to act as active sites for CO gas molecule adsorption. The 2.5%-Au/PANI sensor possessed a high response (14% to 1000 ppm) and low detection limit (33 ppm) for CO gas, which is mainly due to the catalytic properties and high surface energy of Au nanoparticles. As shown in Fig. 9a–c, Chen *et al.*[114] reported core–shell

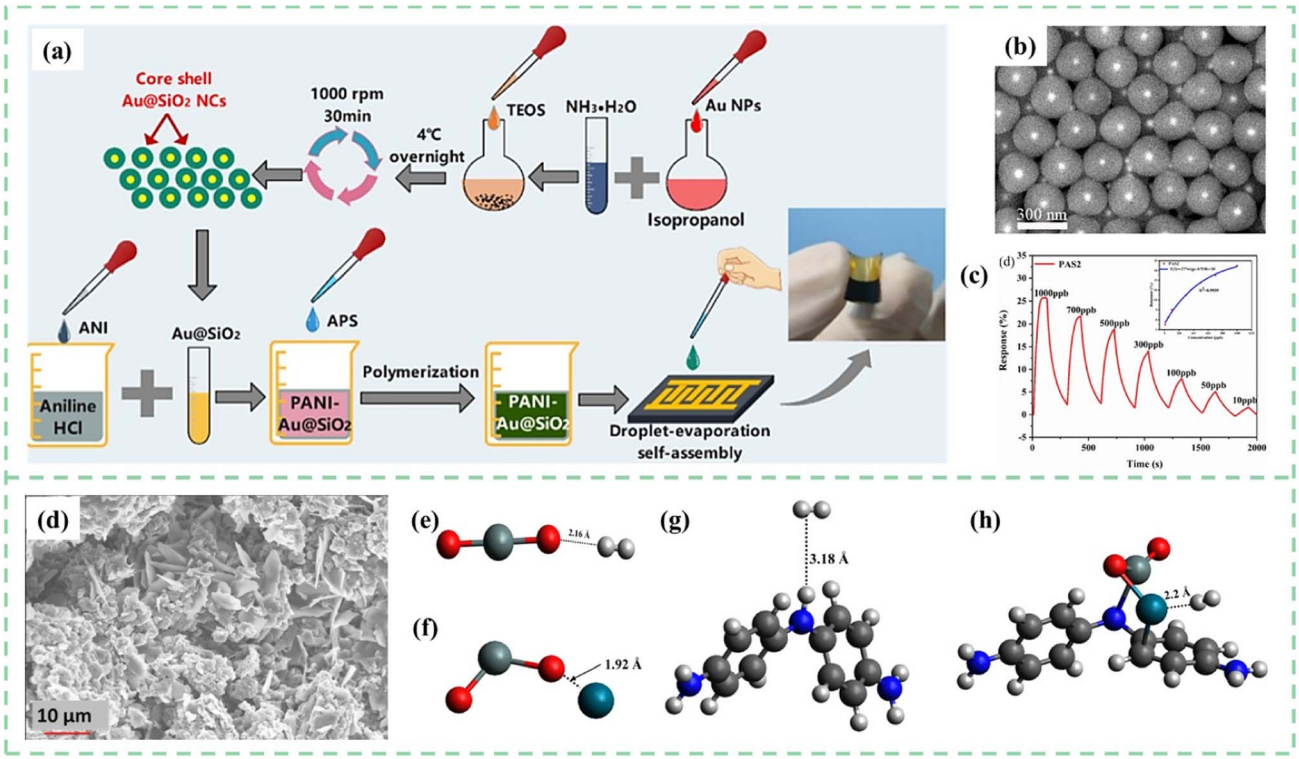

Fig. 9 (a) Schematic illustration of PANI-Au@SiO_2 sensor fabrication. (b) SEM images of the synthesized Au@SiO_2 NCs. (c) Dynamic response recovery of the PANI-Au@SiO_2 sensor to 10–1000 ppb concentration of NH_3. Reproduced from ref. 114 with permission from Elsevier, copyright 2022. (d) SEM images for the prepared films with PANI and Pd doped SnO_2. Interaction of H_2 with (e) SnO_2 (f) SnO_2-Pd (g) PANI and (h) PANI-SnO_2-Pd (black = carbon, grey = hydrogen, red = oxygen, purple = zinc, white = silver, blue = nitrogen, dark blue = palladium). Reproduced from ref. 115 with permission from Elsevier, copyright 2021.

Au@SiO_2 nanocrystal doped PANI materials prepared *via* a simple droplet-evaporation self-assembly process for flexible NH_3 sensors. The fabrication schematic illustration of the PANI-Au@SiO_2 sensor is shown in Fig. 9a. Core–shell microstructure and –OH functional groups distributed on the surface of Au@SiO_2 nanocrystals realized ppb-level NH_3 detection. During this process, small Au NPs with catalytic activity promoted the absorption/desorption of hydrogen atoms.

As shown in Fig. 9d, Pippara *et al.*[115] reported a composite film based on SnO_2 nanosheets with PANI doped with palladium (Pd) fabricated by a hydrothermal synthesis technique. As shown in Fig. 9e–h, DFT calculations were used to obtain the most energetically stable geometry of the sensor and address the adsorption mechanisms of the H_2 gas molecule. Pd acts as a catalyst for the dissociation of H_2 gas molecules into H atoms and forms PdH_x.

4.3. PANI-metal oxide composites

The metal oxides introduced in this section mainly refer to those materials with semiconductor characteristics, including WO_3, CeO_2, SnO_2, ZnO, NiO, Co_3O_4, In_2O_3, V_2O_5, CuO, TiO_2, and so on.[24,116–125] Most metal oxides show obvious gas sensing characteristics, but the working temperature is usually high. After being combined with PANI, the sensitivity, stability, and repeatability of the sensors can be improved. Moreover, the enhancement in sensor performance is primarily attributed to the formation of a p–n junction between metal oxides and PANI.[126]

Tungsten oxide (WO_3) is an n-type semiconductor sensing material with a wide bandgap, which exhibits sensing responses to various toxic gases.[127] However, its main drawbacks include high operating temperature and lack of selectivity for the target gas. As shown in Fig. 10a, Kulkarni *et al.*[128] developed PANI-WO_3 hybrid nanocomposites by an *in situ* chemical oxidative polymerization process on a flexible PET substrate. The impedance spectroscopy technique was used to investigate the interaction between the flexible PANI-WO_3 sensor and the target gas. As shown in Fig. 10b, flexible sensors demonstrated excellent response reproducibility at different bending angles. The PANI-WO_3 hybrid flexible sensor showed a maximum response of 121% and excellent response stability of 83% towards 100 ppm NH_3 gas at room temperature (Fig. 10b and c). Fan *et al.*[129] synthesized WO_3 nanoplates by the intercalation and topochemical conversion process and developed an ultrasonic spray-assisted *in situ* polymerization. WO_3@PANI nanocomposites exhibited a plate-like morphology and the PANI nanocrystals were tightly coated on the WO_3 surfaces. As shown in Fig. 10d–f, the formation of the p–n heterojunction between PANI and WO_3 further enhanced the gas sensitivity. Therefore, the WO_3@PANI nanocomposites exhibited a high response of 34 upon exposure to 100 ppm NH_3 at room temperature.

During the chemical polymerization process of PANI, *in situ* doping is typically conducted in a protonic acid solution environment, which may cause corrosion toward metal oxides.

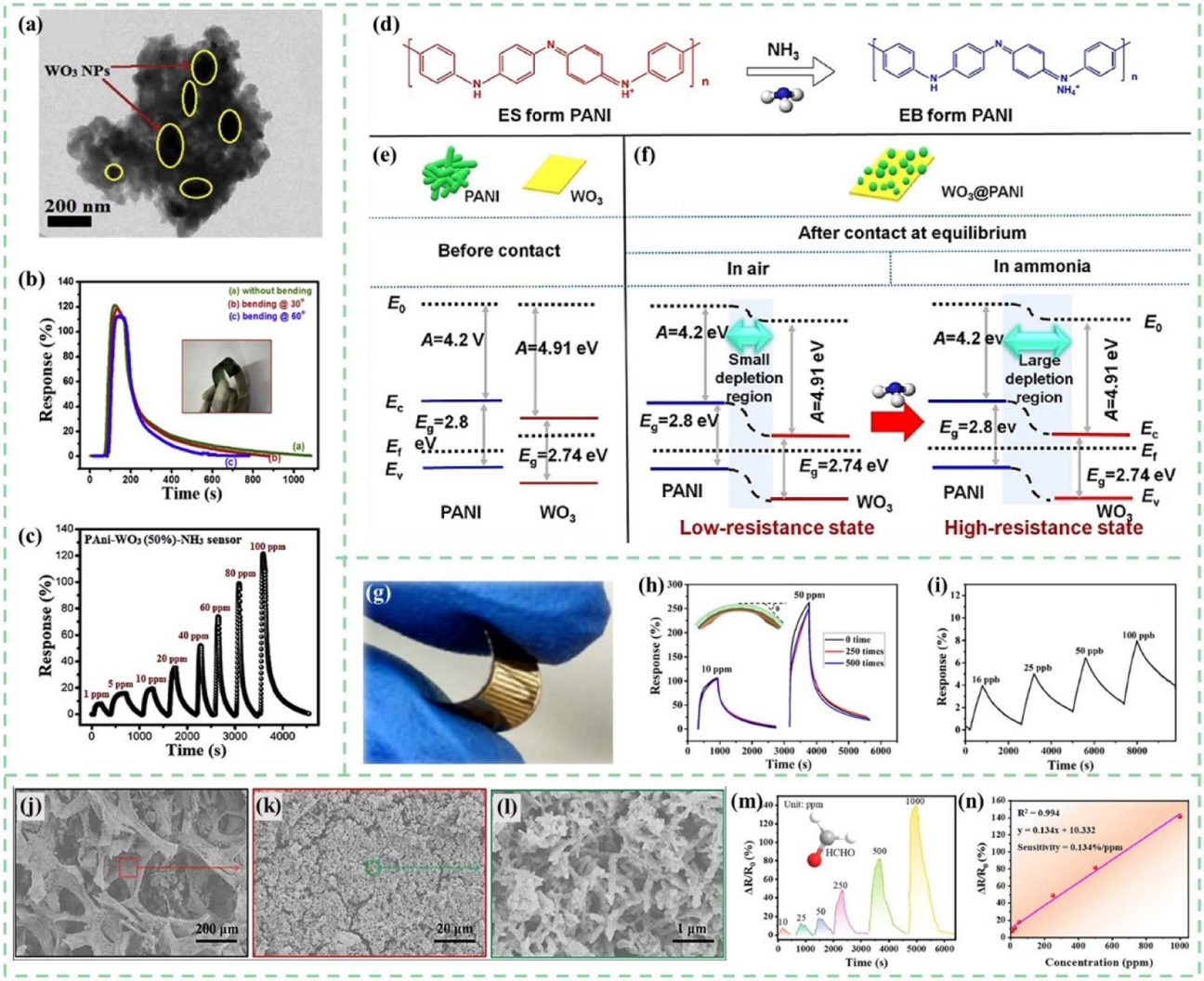

Fig. 10 (a) TEM images of PANI-WO_3 hybrid nanocomposites. (b) Response properties of PANI-WO_3 nanocomposite flexible sensors at different bending angles towards 100 ppm NH_3. (c) Dynamic resistance changes of the flexible PANI-WO_3 hybrid sensor towards 1–100 ppm of NH_3. Reproduced from ref. 128 with permission from Elsevier, copyright 2019. (d) Reaction of PANI and NH_3. (e and f) Energy band diagrams of PANI, WO_3, and the WO_3@PANI heterojunction. Reproduced from ref. 129 with permission from Elsevier, copyright 2020. (g) Photograph of a flexible PANI-CeO_2 sensor. (h) The dynamic resistance changes of the PANI-CeO_2 flexible sensor after different bending cycles towards 10 ppm and 50 ppm NH_3. (i) Response for ultra-low concentration NH_3 of the PANI-CeO_2 film sensor. Reproduced from ref. 130 with permission from Elsevier, copyright 2018. (j–l) SEM images of PANI-ZnO@GPA. (m and n) Changes in the resistance of PANI-ZnO@GPA when exposed to formaldehyde vapor and linear relationship between the response and the concentration. Reproduced from ref. 143 with permission from American Chemical society, copyright 2022.

However, CeO_2 exhibits relatively good corrosion resistance and stability. As shown in Fig. 10g–i, Liu *et al.*[130] prepared a resistive-type flexible ammonia sensor through an *in situ* self-assembly strategy of PANI-CeO_2 on a flexible polyimide substrate. The CeO_2 nanoparticles played a crucial role in constructing the microscopic morphology of composite materials and improving PANI's protonation and oxidation degrees. The PANI-CeO_2 flexible sensors exhibited outstanding chemiresistive characteristics in the presence of ultra-low concentration NH_3 (16 ppb). Liu and Xu *et al.*[131] developed CeO_2@PANI nanomaterials with abundant and stable oxygen vacancies using a straightforward hydrothermal method combined with hydrogen plasma treatment. This treatment generated a significant number of oxygen vacancies on the surface of the CeO_2 and PANI heterostructure, markedly improving the NH_3 response behavior. Compared to the corresponding nanocomposites without hydrogen plasma treatment, the response to 100 ppm NH_3 was significantly heightened, increasing from 165% to 670%, and even achieving a 24% response to as low as 50 ppb NH_3.

SnO_2, an n-type wide band gap semiconductor metal oxide with high mobility of electrons and high chemical and thermal stability, is considered a promising candidate for the fabrication of PANI composite sensors in many research studies.[132–134] To further optimize the sensing performance, some metal particles and carbon nanomaterials are also doped into PANI/SnO_2 sensing composites.[135–137] Aliha *et al.*[138] reported the SnO_2/

PANI nanocomposite material for selective detection of ammonia at room temperature. Different from the traditional deposition method of PANI on SnO_2, a new way of *in situ* deposition–precipitation of SnO_2 on PANI was used in this research. In the synthesis of SnO_2/PANI nanocomposites, the materials were dried at 80 °C for 12 h and then calcined in air at 400 °C for 1.5 h. PANI did not degrade completely even at 400 °C. During heating, PANI crosslinking occurred and the thermal stability of the polymer increased, which made the response of 8 wt% PANI composites 37 times higher than that of pure SnO_2.

As a gas sensing material, PANI/ZnO nanohybrids have also been confirmed to exhibit the advantages of lower detection limits, faster response times, and more stable sensing signals.[139–142] As shown in Fig. 10j–l, Wang *et al.*[143] loaded PANI/ZnO nanohybrids on a self-formed natural grapefruit peel aerogel (GPA) to weaken the agglomeration tendency. The three-dimensional porous structured aerogel sensors could successfully detect formaldehyde at the 10–1000 ppm level and with a sensitivity of 0.134% ppm^{-1} (Fig. 10m and n).

In addition, the doping of Ag_2O in PANI can enhance the selectivity and sensitivity of the sensor. Farea *et al.*[144] used *in situ* polymerization technology to prepare Ag_2O-doped PANI composite materials. The incorporation of Ag_2O nanoparticles into PANI significantly increased the response rate (97% for 500 ppm) and reduced the response and recovery times (37 s/41 s) of the sensor.

4.4. PANI-metal sulfide composites

The mechanism of metal sulfides enhancing the gas sensing performance of PANI is similar to that of metal oxides. They can form heterojunctions with PANI, thereby improving the gas sensing performance. Additionally, the improvement in sensing performance can be attributed to the fact that transition metal dichalcogenides (TMDs) mostly possess a two-dimensional layered structure, which has the advantages of a large surface-to-volume ratio, nanoscale thickness, easy surface functionalization, and excellent device integration compatibility.[145]

For example, molybdenum disulfide (MoS_2), as a typical TMD, has good gas-sensitive properties, but the sheet layer tends to form a tightly stacked structure during the formation of gas-sensitive networks, which is not conducive to sufficient contact between MoS_2 and the gas molecule. To solve the above problems, Liu *et al.*[146] prepared PANI/MoS_2 nanosheets/SnO_2 nanotubes *via* electrostatic spinning, a hydrothermal route, and an *in situ* polymerization technique for the room temperature detection of ammonia. Due to the energy-gap difference between the PANI and MoS_2 species, a p–n heterojunction can be formed at the interface between the n-type MoS_2 nanoplates and p-type PANI nanocrystals. When PANI/MoS_2/SnO_2 came in contact with ammonia molecules, NH_3 captured the proton from PANI and further widened the depletion layer. In addition, electrospun SnO_2 hollow nanotubes prevented the stacking of MoS_2 and provided a high specific surface area. The gas sensor exhibited a response signal of 10.9 towards 100 ppm NH_3 at room temperature and a low detection limit of 200 ppb.

Liu *et al.*[147] prepared a porous PANI/WS_2 nanocomposite film to detect ppm-level NH_3 gas under a humid atmosphere. The performance of the PANI/WS_2 sensor was related to the content of WS_2. Through intentional adjustment of the WS_2 loading (1.5 mg), the PANI/WS_2 sensor showed an improvement in the sensing response, response–recovery feature, and operational robustness.

In addition, CdS is a direct band gap II–VI semiconductor with a band gap of 2.42 eV at room temperature. Akbar *et al.*[148] provided a chemical co-dispersion technique to develop CdS decorated PANI nanocomposites for NH_3 detection. The PANI/CdS sensor showed a much faster recovery speed compared to pure PANI.

4.5. PANI-MXene composites

MXenes, a new two-dimensional inorganic compound discovered in 2011, are generally composed of transition metal carbides, nitrides, or carbonitrides with a thickness of several atomic layers. It is usually synthesized by selectively etching the group A element from the MAX phase compound, where M represents the transition metal, X represents carbon or nitrogen, and the group A element can include aluminum, gallium, silicon, and other elements. Due to the presence of hydroxyl or terminal oxygen on the surface of MXene materials, they have the metal conductivity of transition metal carbides. MXenes have been widely used in fields such as humidity sensing, energy storage, and solid-state batteries.[149,150]

The composite of PANI or other conducting polymers with MXenes to form nanocomposites is an effective strategy for the preparation of high-performance gas sensors.[89] In addition, the formation of heterojunctions or Schottky junctions at the interface of MXenes and PANI is the reason for the improvement in gas sensor sensitivity.[151]

$Ti_3C_2T_x$, a common MXene material, is a promising candidate for PANI/MXenes gas sensors.[152,153] As shown in Fig. 11a and b, PANI/$Ti_3C_2T_x$ hybrid sensitive films were synthesized on flexible Au interdigital electrodes (IDEs) by an *in situ* self-assembly method and successfully employed for sensing ammonia gas by Li *et al.*[154] PANI doped with protonic acid had a higher work function than $Ti_3C_2T_x$. PANI combined with $Ti_3C_2T_x$ to form Schottky junctions with hole depletion regions at the interfaces. Therefore, when exposed to NH_3, the conductivity of PANI decreased and the conduction pathway became narrower. The sensor exhibited excellent NH_3-sensing properties in 20–80% relative humidity (RH) environments at a temperature range of 10–40 °C. Furthermore, the hybrid sensor on the PI substrate shows excellent mechanical flexibility properties shown in Fig. 11c. Wen *et al.*[155] fabricated PANI:PSS/$Ti_3C_2T_x$ composites for conductometric flexible ammonia gas sensors. Similarly, the formation of the Schottky junction at the interface between PANI:PSS and $Ti_3C_2T_x$ improved gas sensing performances for these film sensors.

Furthermore, layered MXenes have unique structural properties and conductive mechanisms for gas sensing. When MXenes are exposed to target gases, changes in their conductivity occur due to interlayer expansion caused by gas molecule

insertion between layers. The resistance of the interlayer expanded MXenes will increase due to the blocked electron transport outside the surface. This effect is similar to the trend of resistance change of PANI in a target gas atmosphere. Therefore, Wang *et al.*[156,157] proposed PANI nanofiber-supported Nb_2CT_x nanosheets to detect environment/breath NH_3 at room temperature. As shown in Fig. 11d, the ultrathin 2D Nb_2CT_x nanosheets were synthesized through hydrofluoric acid (HF) etching and the tetrapropylammonium hydroxide (TPAOH) intercalation process. As shown in Fig. 11e, a depletion layer formed at the heterojunction interface between PANI and Nb_2CT_x. The thickness of the depletion

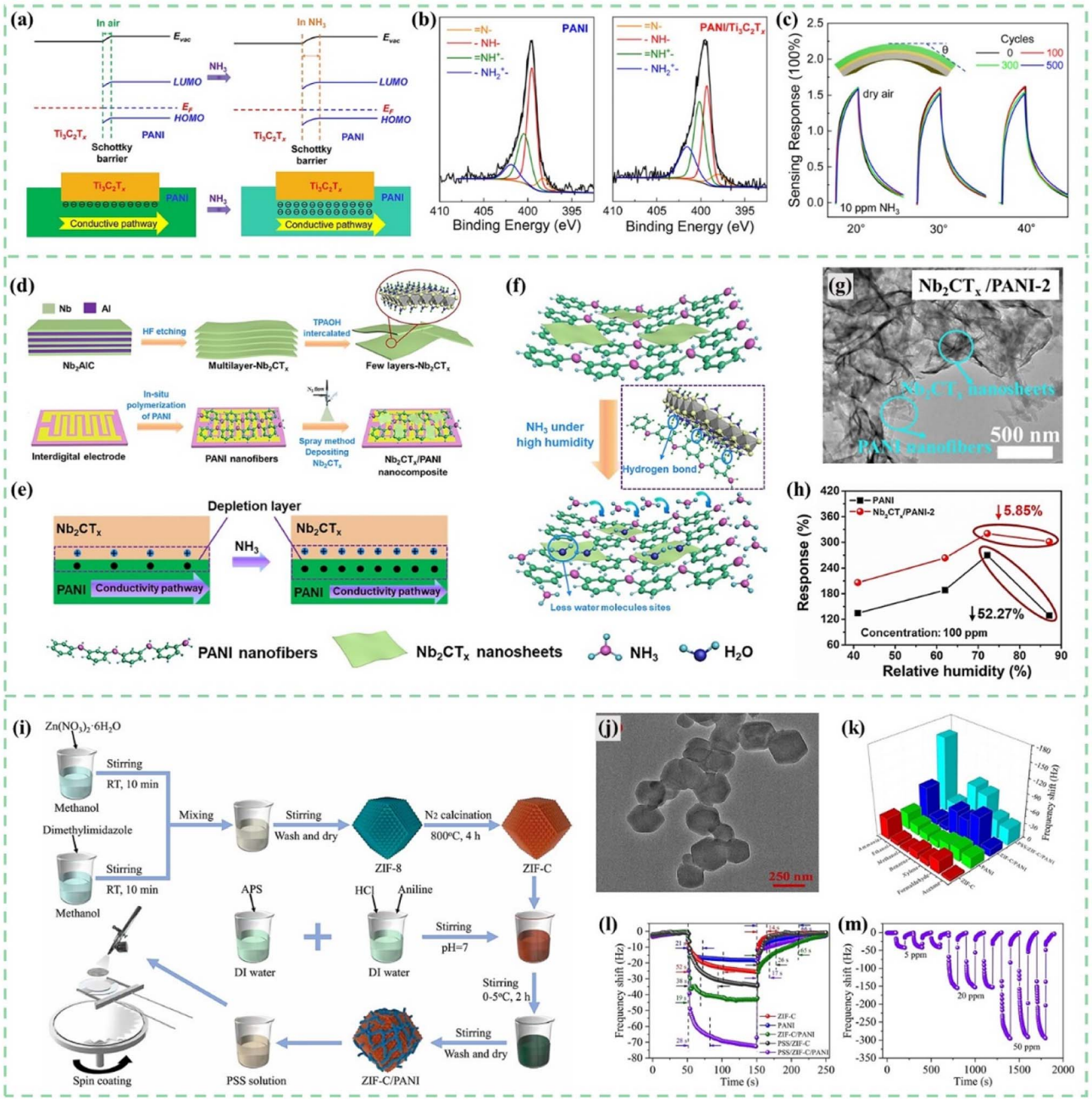

Fig. 11 (a) Energy level alignments and conductivity pathway of the hybrid PANI/$Ti_3C_2T_x$ sensitive films before and after NH_3 molecule absorption. (b) XPS N 1s spectrum of PANI/$Ti_3C_2T_x$. (c) Stability test of the PANI/$Ti_3C_2T_x$ flexible sensor under different bending angles and after different bending times. Reproduced from ref. 154 with permission from Elsevier, copyright 2020. (d) Synthesis process of the ultrathin 2D Nb_2CT_x nanosheets. (e) Depletion layer and conductivity pathway changes of the Nb_2CT_x/PANI film before and after NH_3 adsorption. (f–h) Gas sensing mechanism, morphology, and humidity influence of the Nb_2CT_x/PANI sensor for high humid NH_3 detection. Reproduced from ref. 156 with permission from Elsevier, copyright 2021. (i and j) Schematic diagram of the preparation process and TEM images of PSS/ZIF-C/PANI. (k–m) Selectivity, response/recovery time and repeatability of the PSS/ZIF-C/PANI sensor. Reproduced from ref. 161 with permission from Elsevier, copyright 2022.

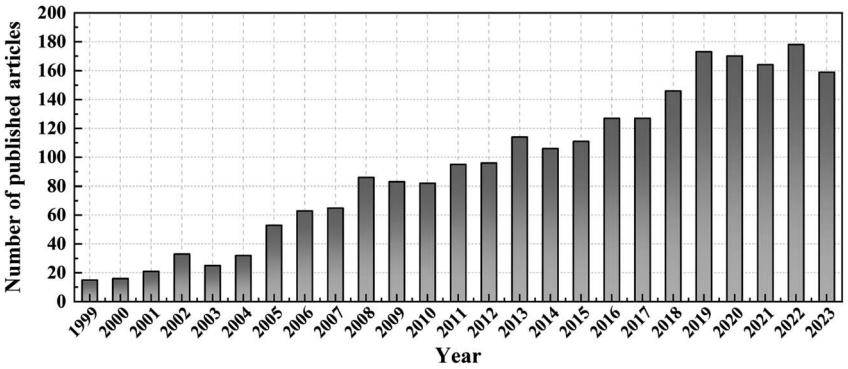

Fig. 12 A year-by-year increase in the number of publications on PANI gas sensors in 1999–2023 (Source: Web of Science, Search key: PANI gas sensors or polyaniline gas sensors).

layer will be significantly affected by the ammonia concentration in the surrounding environment. As shown in Fig. 11f–h, the hydrogen bonds between Nb_2CT_x nanosheets and PANI would also be helpful to reduce the active sites for water molecules, which will improve the sensing performance of the Nb_2CT_x/PANI sensor in a high humidity environment.

4.6. PANI-MOF composites

Metal–organic frameworks (MOFs) are a new class of organic–inorganic hybrid crystalline porous coordination polymers composed of positively charged metal ions connected with organic ligands, which have outstanding features such as high porosity, adjustable structure, and easy modification. Furthermore, their structure and functionality can be adjusted through molecular modification. As a result, gas molecules can be selectively adsorbed onto the active sites of MOFs.[158] A strong interfacial interaction between MOFs and PANI dramatically enhances gas sensing performance. Additionally, the composite material alleviates the issues of poor chemical stability and dispersion of MOF materials.[158]

Mashao *et al.*[159] developed PANI doped with a cobalt-based zeolitic benzimidazolate framework material (CoZIF). The PANI-CoZIF metal–organic framework composite material was applied in electrochemical hydrogen gas sensing. The composites showed high sensitivity and fast response time, while they can be used as an electrocatalytic material for hydrogen production *via* the hydrogen evolution reaction (HER).

Lin *et al.*[160] fabricated a microchannel tube NH_3 sensor based on PANI modified with UiO-66 MOFs *via* a dynamic liquid deposition method. By improving the hydrophilicity of aniline oligomers, the additive of UiO-66 induced the formation of a porous structure. The gas sensing response of PANI/UiO-66 nanofibres increased up to 25.4 for 100 ppm NH_3 and 20% for 10 ppb NH_3. The composites also exhibit excellent reversibility and a fast response/recovery time (25 s/14 s).

As shown in Fig. 11i and j, Zhang *et al.*[161] synthesized PSS/ZIF-C/PANI composites *via* MOF template-carbonization and *in situ* polymerization for ammonia gas detection. The adsorption sites and voids in the unique porous carbon structure derived from ZIF-8 provided support for PANI and PSS anion chains, which was conducive to the complete contact of target gas molecules with the sensing film and accelerated the adsorption/desorption rate. Sensors showed high response/recovery capability (28 s/17 s) (Fig. 11k–m).

5. Conclusions and perspectives

PANI and its composite materials show huge development potential in the field of gas sensing. In this paper, the gas sensing mechanism of chemiresistive PANI and heterojunction-based PANl composites is first introduced. Nanomaterials exhibit a high surface area ratio, which makes nano gas-sensitive materials exhibit excellent gas sensing properties. This paper reviews the synthesis methods and manufacturing processes of 0D, 1D, 2D, and 3D PANI and their composites. Nano gas-sensitive materials possessed faster response/recovery time, relatively steady response/recovery curves, remarkable durability and reproducibility, and ultra-low detection limits. Subsequently, this article summarises the sensors of hybrid materials composed of PANI and carbon materials, metals, metal oxides, metal sulfides, MXenes, MOFs, *etc.* The review illustrates a variety of preparation methods for PANI composite materials. Many ingenious designs of PANI gas sensors, such as the construction of three-dimensional nanostructures or the formation of heterojunctions between composite materials, are thought to significantly improve gas sensing performance. The number of articles published on PANI gas sensors has gradually increased since 1999 (Fig. 12).

Based on the aforementioned advantages, PANI composite materials exhibit substantial application potential in several areas:

1. Detection of toxic and hazardous gases, preventing harm to human health from gas leaks or environmental pollution.

2. Monitoring exhaled gases related to human diseases, such as renal diseases, facilitating early detection or prevention of the diseases.

3. Sensing humidity or carbon dioxide, enabling real-time monitoring of human activity and physiological states.

However, polyaniline gas sensors still face numerous technical challenges that need to be overcome:

1. From the perspective of material synthesis, the research on the synthesis of soluble PANI derivatives still needs to be carried out.

2. Addressing the issue of diminished sensitivity in sensors operating under high-temperature and high-humidity conditions is crucial. This advancement is key to achieving stable sensor performance in complex environmental settings.

3. Developing PANI gas sensors for gases other than NH_3. For instance, the sensitivity of PANI composites towards gases like CO and H_2S is significantly lower compared to NH_3. Enhancing this sensitivity can broaden the application scope of PANI composite material gas sensors.

4. Addressing the problem of performance degradation of PANI gas sensors after long-term exposure to the environment, including both the reduction in sensor repeatability and the natural degradation of sensor performance.

5. The integration of PANI sensors with other types of sensors is also a critical area for development. This includes the integration of PANI sensors with various gas sensors, as well as with other sensor types, such as stress sensors, temperature sensors, and proximity sensors. Furthermore, integrating PANI gas sensors with energy devices for self-powering and wireless signal transmission is also an urgent research direction.

More research is needed in these areas.

Author contributions

Jiayue Wen, investigation, writing – original draft. Shang Wang, review & editing. Jiayun Feng, review & editing. Jingxuan Ma, review & editing. He Zhang, review & editing. Peng Wu, review & editing. Geng Li, review & editing. Zhuohuan Wu, review & editing. Fanzhou Meng, review & editing. Longqiu Li, review & editing. Yanhong Tian, review & editing, supervision, funding acquisition.

Conflicts of interest

The authors declare that they have no known competing financial interests or personal relationships that could have appeared to influence the work reported in this paper.

Acknowledgements

This work was supported by the National Natural Science Foundation of China (Grant No. 52175300), Heilongjiang Province Key Research and Development Program under Grant No. 2022XJ03C07, Fundamental Research Funds for the Central Universities (2022FRFK060008), and Heilongjiang Touyan Innovation Team Program (HITTY-20190013).

References

1 *Billions of people still breathe unhealthy air: new WHO data*, 2022, **https://www.who.int/news/item/04-04-2022-billions-of-people-still-breathe-unhealthy-air-new-who-data**, accessed April.
2 C.-T. Lee and Y.-S. Wang, *J. Alloys Compd.*, 2019, **789**, 693–696.
3 Y. Li, Y. Li, J. Shi, Z. Li, X. Wang, X. Hu, Y. Gong and X. Zou, *Foods*, 2022, **11**, 2372.
4 C. Pi, W. Chen, W. Zhou, S. Yan, Z. Liu, C. Wang, Q. Guo, J. Qiu, X. Yu, B. Liu and X. Xu, *J. Mater. Chem. C*, 2021, **9**, 11299–11305.
5 T. Seiyama, A. Kato, K. Fujiishi and M. Nagatani, *Anal. Chem.*, 1962, **34**, 1502–1503.
6 C. Lou, G. Lei, X. Liu, J. Xie, Z. Li, W. Zheng, N. Goel, M. Kumar and J. Zhang, *Coord. Chem. Rev.*, 2022, **452**, 214280.
7 C. Lou, K. Wang, H. Mei, J. Xie, W. Zheng, X. Liu and J. Zhang, *CrystEngComm*, 2021, **23**, 3654–3663.
8 Y. Wang, A. Liu, Y. Han and T. Li, *Polym. Int.*, 2020, **69**, 7–17.
9 S. Iqbal and S. Ahmad, *J. Ind. Eng. Chem.*, 2018, **60**, 53–84.
10 M. Das and S. Roy, *Mater. Sci. Semicond. Process.*, 2021, **121**, 105332.
11 Y. C. Wong, B. C. Ang, A. S. M. A. Haseeb, A. A. Baharuddin and Y. H. Wong, *J. Electrochem. Soc.*, 2019, **167**, 037503.
12 B. Li, Y. Li and P. Ma, *Org. Electron.*, 2023, **114**, 106749.
13 D. Lv, W. Shen, W. Chen, Y. Wang, R. Tan, M. Zhao and W. Song, *Sens. Actuator A Phys.*, 2023, **350**, 114120.
14 C. Zhu, X. Dong, C. Guo, L. Huo, S. Gao, Z. Zheng, X. Cheng and Y. Xu, *J. Mater. Chem. A*, 2022, **10**, 12150–12156.
15 I. Fratoddi, I. Venditti, C. Cametti and M. V. Russo, *Sens. Actuators B Chem.*, 2015, **220**, 534–548.
16 A. G. Macdiarmid, J. C. Chiang, A. F. Richter and A. J. Epstein, *Synth. Met.*, 1987, **18**, 285–290.
17 E. Song and J.-W. Choi, *Nanomaterials*, 2013, **3**, 498–523.
18 S. Li, A. Liu, Z. Yang, J. He, J. Wang, F. Liu, H. Lu, X. Yan, P. Sun, X. Liang, Y. Gao and G. Lu, *Sens. Actuators B Chem.*, 2019, **299**, 126970.
19 J. Huang, S. Virji, B. H. Weiller and R. B. Kaner, *Chem.–Eur. J.*, 2004, **10**, 1314–1319.
20 J. Dai, O. Ogbeide, N. Macadam, Q. Sun, W. Yu, Y. Li, B.-L. Su, T. Hasan, X. Huang and W. Huang, *Chem. Soc. Rev.*, 2020, **49**, 1756–1789.
21 M. A. Farea, H. Y. Mohammed, S. M. Shirsat, P. W. Sayyad, N. N. Ingle, T. Al-Gahouari, M. M. Mahadik, G. A. Bodkhe and M. D. Shirsat, *Chem. Phys. Lett.*, 2021, **776**, 138703.
22 X. Liu, W. Zheng, R. Kumar, M. Kumar and J. Zhang, *Coord. Chem. Rev.*, 2022, **462**, 214517.
23 D. Han, X. Han, X. Liu, J. Zhang, L. Zhao, X. He, W. Wang, B. Xu and S. Sang, *Sens. Actuators B Chem.*, 2023, **385**, 133688.
24 J. N. O. Amu-Darko, S. Hussain, Q. Gong, X. Zhang, Z. Xu, M. Wang, G. Liu and G. Qiao, *J. Environ. Chem. Eng.*, 2023, **11**, 109211.
25 Z. Pang, E. Yildirim, M. A. Pasquinelli and Q. Wei, *ACS Omega*, 2021, **6**, 8950–8957.
26 M. Matsuguchi, T. Nakamae, R. Fujisada and S. Shiba, *Sensors*, 2021, **21**, 7522.
27 M. G. Han, S. K. Cho, S. G. Oh and S. S. Im, *Synth. Met.*, 2002, **126**, 53–60.
28 K. Crowley, A. Morrin, A. Hernandez, E. O'Malley, P. G. Whitten, G. G. Wallace, M. R. Smyth and A. J. Killard, *Talanta*, 2008, **77**, 710–717.

29 C. Fisher, B. J. Warmack, Y. Yu, L. N. Skolrood, K. Li, P. C. Joshi, T. Saito and T. Aytug, *J. Mater. Sci.*, 2021, **56**, 12596–12606.
30 J. C. Bittencourt, B. H. de Santana Gois, V. J. Rodrigues de Oliveira, D. L. da Silva Agostini and C. de Almeida Olivati, *J. Appl. Polym. Sci.*, 2019, **136**, 47288.
31 J. Wen, Y. Tian, C. Hao, S. Wang, Z. Mei, W. Wu, J. Lu, Z. Zheng and Y. Tian, *J. Mater. Chem. C*, 2019, **7**, 1188–1197.
32 S. B. Kulkarni, Y. H. Navale, S. T. Navale, F. J. Stadler and V. B. Patil, *J. Mater. Sci.: Mater. Electron.*, 2019, **30**, 8371–8380.
33 R. Kashyap, R. Kumar, M. Kumar, S. Tyagi and D. Kumar, *Mater. Res. Express*, 2019, **6**, 1150d3.
34 X.-X. Wang, G.-F. Yu, J. Zhang, M. Yu, S. Ramakrishna and Y.-Z. Long, *Prog. Mater. Sci.*, 2021, **115**, 100704.
35 V. Kumar, A. Mirzaei, M. Bonyani, K.-H. Kim, H. W. Kim and S. S. Kim, *TrAC, Trends Anal. Chem.*, 2020, **129**, 115938.
36 N. D. Sonwane and S. B. Kondawar, *Synth. Met.*, 2022, **284**, 117004.
37 G. Wu, H. Du, K. Pakravan, W. Kim, Y. L. Cha, S.-T. Chiang, M. Beidaghi, X. Zhang, S. H. Kim, X. Pan and D.-J. Kim, *Chem. Eng. J.*, 2023, **475**, 146228.
38 A. Korent, K. Žagar Soderžnik, S. Šturm, K. Žužek Rožman, N. Redon, J.-L. Wojkiewicz and C. Duc, *Sensors*, 2021, **21**, 169.
39 A. Popov, B. Brasiunas, L. Mikoliunaite, G. Bagdziunas, A. Ramanavicius and A. Ramanaviciene, *Polymer*, 2019, **172**, 133–141.
40 S. Saad Ali, A. Pauly, J. Brunet, C. Varenne and A. L. Ndiaye, *Sens. Actuators B Chem.*, 2020, **320**, 128364.
41 H. Abu Hassan Shaari, M. M. Ramli, M. N. Mohtar, N. Abdul Rahman and A. Ahmad, *Polymers*, 2021, **13**, 1939.
42 P. B. D. Firda and J.-W. Jeon, *ACS Appl. Polym. Mater.*, 2022, **4**, 4850–4859.
43 A. M. Graboski, E. Galvagni, A. Manzoli, F. M. Shimizu, C. A. Zakrzevski, T. A. Weschenfelder, J. Steffens and C. Steffens, *Food Res. Int.*, 2018, **113**, 309–315.
44 C. Zhu, Y. Xu, T. Zhou, L. Liu, Q. Chen, B. Gao and T. Zhang, *Sens. Actuators B Chem.*, 2022, **365**, 131928.
45 T. Zhang, H. Qi, Z. Liao, Y. D. Horev, L. A. Panes-Ruiz, P. S. Petkov, Z. Zhang, R. Shivhare, P. Zhang, K. Liu, V. Bezugly, S. Liu, Z. Zheng, S. Mannsfeld, T. Heine, G. Cuniberti, H. Haick, E. Zschech, U. Kaiser, R. Dong and X. Feng, *Nat. Commun.*, 2019, **10**, 4225.
46 H. Wang, S. Nie, H. Li, R. Ali, J. Fu, H. Xiong, J. Li, Z. Wu, W.-M. Lau, N. Mahmood, R. Jia, Y. Liu and X. Jian, *ACS Sens.*, 2019, **4**, 2343–2350.
47 L. Wang, H. Fu, H. Liu, K. Yu, Y. Wang and J. Ma, *Mater. Res. Bull.*, 2018, **107**, 46–53.
48 S. Li, P. Lin, L. Zhao, C. Wang, D. Liu, F. Liu, P. Sun, X. Liang, F. Liu, X. Yan, Y. Gao and G. Lu, *Sens. Actuators B Chem.*, 2018, **259**, 505–513.
49 L. Yang, X. Xu, M. Liu, C. Chen, J. Cui, X. Chen, K. Wu and D. Sun, *Sens. Actuators B Chem.*, 2021, **334**, 129647.
50 J. Bhadra, A. Popelka, A. Abdulkareem, Z. Ahmad, F. Touati and N. Al-Thani, *RSC Adv.*, 2019, **9**, 12496–12506.
51 A. M. Safe, F. Ahmadi Tabar, A. Nikfarjam, F. Sharif, H. Hajghassem and S. Mazinani, *IEEE Sens. J.*, 2019, **19**, 9616–9623.
52 F. Ahmadi Tabr, F. Salehiravesh, H. Adelnia, J. N. Gavgani and M. Mahyari, *Talanta*, 2019, **197**, 457–464.
53 S. Tohidi, M. Parhizkar, H. Bidadi and R. Mohamad-Rezaei, *Nanotechnology*, 2020, **31**, 415501.
54 J. Chang, X. Zhang, Z. Wang, C. Li, Q. Hu, J. Gao and L. Feng, *ACS Appl. Nano Mater.*, 2021, **4**, 5263–5272.
55 S.-Z. Hong, Q.-Y. Huang and T.-M. Wu, *Polymers*, 2021, **13**, 3676.
56 G. Wu, H. Du, Y. L. Cha, D. Lee, W. Kim, F. Feyzbar-Khalkhali-Nejad, T.-S. Oh, X. Zhang and D.-J. Kim, *Sens. Actuators B Chem.*, 2023, **375**, 132858.
57 W. Zhang, S. Cao, Z. Wu, M. Zhang, Y. Cao, J. Guo, F. Zhong, H. Duan and D. Jia, *Sensors*, 2020, **20**, 149.
58 C. Zhu, T. Zhou, H. Xia and T. Zhang, *Nanomaterials*, 2023, **13**, 1158.
59 N. Bafandeh, M. M. Larijani and A. Shafiekhani, *Polym. Bull.*, 2020, **77**, 3697–3706.
60 D. Maity and R. T. R. Kumar, *ACS Sens.*, 2018, **3**, 1822–1830.
61 M. Eising, C. E. Cava, R. V. Salvatierra, A. J. G. Zarbin and L. S. Roman, *Sens. Actuators B Chem.*, 2017, **245**, 25–33.
62 L. Kumar, I. Rawal, A. Kaur and S. Annapoorni, *Sens. Actuators B Chem.*, 2017, **240**, 408–416.
63 M. Kumar, S. Sharma, R. Pal, B. Vidhani and Supreet, *Sens. Actuator A Phys.*, 2023, **353**, 114210.
64 S.-Z. Hong, Q.-Y. Huang and T.-M. Wu, *Sensors*, 2022, **22**, 1570.
65 C. Liu, H. Tai, P. Zhang, Z. Ye, Y. Su and Y. Jiang, *Sens. Actuators B Chem.*, 2017, **246**, 85–95.
66 A. Jia, B. Liu, H. Liu, Q. Li and Y. Yun, *Front. Chem.*, 2020, **8**, 383.
67 N. D. Sonwane, M. D. Maity and S. B. Kondawar, *Mater. Today: Proc.*, 2019, **15**, 447–453.
68 L. Guo, W. Liu and C. Wang, *Appl. Surf. Sci.*, 2023, **630**, 157529.
69 S. Jain, N. Karmakar, A. Shah and N. G. Shimpi, *Mater. Sci. Eng., B*, 2019, **247**, 114381.
70 R. K. Sonker, B. C. Yadav, A. Sharma, M. Tomar and V. Gupta, *RSC Adv.*, 2016, **6**, 56149–56158.
71 N. Karmakar, S. Jain, R. Fernandes, A. Shah, U. Patil, N. Shimpi and D. Kothari, *ChemistrySelect*, 2023, **8**, e202204284.
72 D. Selvakumar, K. P. Sonu, G. Ramadoss, R. Sivaramakrishnan, R. Jayavel, M. Eswaramoorthy, K. Venkateswara Rao and A. Pugazhendhi, *Chemosphere*, 2023, **314**, 137492.
73 T. Tohidi, S. Tohidi and R. Mohammad-Rezaei, *J. Mater. Sci.: Mater. Electron.*, 2020, **31**, 19119–19129.
74 R. K. Sonker and B. C. Yadav, *J. Taiwan Inst. Chem. Eng.*, 2017, **77**, 276–281.
75 Y. Li, H. Zhao, H. Ban and M. Yang, *Sens. Actuators B Chem.*, 2017, **245**, 34–43.
76 R. S. Andre, F. M. Shimizu, C. M. Miyazaki, A. Riul, D. Manzani, S. J. L. Ribeiro, O. N. Oliveira,

L. H. C. Mattoso and D. S. Correa, *Sens. Actuators B Chem.*, 2017, **238**, 795–801.
77 X. Wang, L. Gong, D. Zhang, X. Fan, Y. Jin and L. Guo, *Sens. Actuators B Chem.*, 2020, **322**, 128615.
78 S. Li, A. Liu, Z. Yang, L. Zhao, J. Wang, F. Liu, R. You, J. He, C. Wang, X. Yan, P. Sun, X. Liang and G. Lu, *Sens. Actuators B Chem.*, 2019, **289**, 252–259.
79 W. He, Y. Zhao and Y. Xiong, *ACS Omega*, 2020, **5**, 9744–9751.
80 V. Chaudhary, R. K. Talreja, Sonu, S. Rustagi, R. Walvekar and A. Gautam, *Int. J. Hydrog. Energy*, 2024, **52**, 1156–1163.
81 R. N. Dhanawade, N. S. Pawar, M. A. Chougule, G. M. Hingangavkar, T. M. Nimbalkar, G. T. Chavan, C.-W. Jeon and V. B. Patil, *ChemistrySelect*, 2023, **8**, e202204750.
82 C. Zhu, X. Cheng, X. Dong and Y. M. Xu, *Front. Chem.*, 2018, **6**, 493.
83 A. Sunilkumar, B. S. Khened, B. Chethan, V. Prasad, M. G. Kotresh, T. M. Sharanakumar and V. S. Veena, *Inorg. Chem. Commun.*, 2023, **150**, 110476.
84 B. Zhang, F. Shang, X. Shi, R. Yao, F. Wei, X. Hou, W. Li and J. Zhang, *ACS Appl. Nano Mater.*, 2023, **6**, 18413–18425.
85 H. Parangusan, J. Bhadra, R. A. Al-Qudah, E. C. Elhadrami and N. J. Al-Thani, *Nanomaterials*, 2022, **12**, 4423.
86 X. Tian, X. Cui, Y. Xiao, T. Chen, X. Xiao and Y. Wang, *ACS Appl. Mater. Interfaces*, 2023, **15**, 9604–9617.
87 R. K. Jha, M. Wan, C. Jacob and P. K. Guha, *New J. Chem.*, 2017, **42**, 735–745.
88 Z. Wu, L. Liang, S. Zhu, Y. Guo, Y. Yao, Y. Yang, S. Gu and Z. Zhou, *Nanomaterials*, 2021, **11**, 3026.
89 L. Zhao, K. Wang, W. Wei, L. Wang and W. Han, *InfoMat*, 2019, **1**, 407–416.
90 R. Yang, J. Zhang, J. Liu, G. Li, Y. Qiao, X. Zhang, J. Gao and H. Lu, *Sens. Actuators B Chem.*, 2023, 134128.
91 X. Wang, D. Zhang, H. Zhang, L. Gong, Y. Yang, W. Zhao, S. Yu, Y. Yin and D. Sun, *Nano Energy*, 2021, **88**, 106242.
92 P. Li, H. Xu, F. Liu, J. Shi, X. Gao and J. Li, *ACS Appl. Nano Mater.*, 2023, **6**, 5145–5154.
93 M. Khalifa and S. Anandhan, *Nanotechnology*, 2021, **32**, 485504.
94 A. Liu, C. Wang, X. Yang, F. Liu, S. Li, J. Wang, R. You, Z. Yang, J. He, L. Jiang, X. Yan, P. Sun and G. Lu, *Sens. Actuators B Chem.*, 2020, **317**, 128218.
95 D. Zhang, Y. Yang, Z. Xu, D. Wang and C. Du, *J. Mater. Chem. A*, 2022, **10**, 10935–10949.
96 N. D. Sonwane and S. B. Kondawar, *Mater. Lett.*, 2021, **303**, 130566.
97 S. Mousavi, K. Kang, J. Park and I. Park, *RSC Adv.*, 2016, **6**, 104131–104138.
98 F. S. Hadano, A. E. X. Gavim, J. C. Stefanelo, S. L. Gusso, A. G. Macedo, P. C. Rodrigues, A. R. bin Mohd Yusoff, F. K. Schneider, J. F. de Deus and W. José da Silva, *Sensors*, 2021, **21**, 4947.
99 Y. Yuan, H. Wu, X. Bu, Q. Wu, X. Wang, C. Han, X. Li, X. Wang and W. Liu, *Materials*, 2021, **14**, 2829.
100 G. Wu, H. Du, D. Lee, Y. L. Cha, W. Kim, X. Zhang and D.-J. Kim, *ACS Appl. Mater. Interfaces*, 2022, **14**, 56056–56064.
101 C. Wu, L. Han, J. Zhang, Y. Wang, R. Wang and L. Chen, *Adv. Mater. Technol.*, 2022, **7**, 2101247.
102 X. Chen, X. Chen, X. Ding, X. Yu and X. Yu, *IEEE Sens. J.*, 2022, **22**, 1905–1915.
103 Z. Wang, J. Chang, H. Zhi, C. Li and L. Feng, *Sens. Actuators B Chem.*, 2022, **356**, 131292.
104 A. Umar, A. A. Ibrahim, H. Algadi, H. Albargi, M. A. Alsairi, Y. Wang and S. Akbar, *Ceram. Int.*, 2021, **47**, 25696–25707.
105 G. Luo, L. Xie, M. He, R. Jaisutti and Z. Zhu, *Nanotechnology*, 2021, **32**, 305501.
106 D. Zhang, Z. Wu and X. Zong, *Sens. Actuators B Chem.*, 2019, **289**, 32–41.
107 A. Singh, P. Dipak, A. Iqbal, A. Samadhiya, S. K. Dwivedi, D. C. Tiwari, R. K. Tiwari and K. N. Pandey, *Sci. Rep.*, 2023, **13**, 8074.
108 M. M. Rana, D. S. Ibrahim, M. R. Mohd Asyraf, S. Jarin and A. Tomal, *Sens. Rev.*, 2017, **37**, 127–136.
109 A. Roy, A. Ray, P. Sadhukhan, K. Naskar, G. Lal, R. Bhar, C. Sinha and S. Das, *Synth. Met.*, 2018, **245**, 182–189.
110 J. Ma, H. Fan, Z. Li, Y. Jia, A. K. Yadav, G. Dong, W. Wang, W. Dong and S. Wang, *Sens. Actuators B Chem.*, 2021, **334**, 129677.
111 V. Mooss, Y. Kesari and A. Athawale, *J. Mater. NanoSci.*, 2022, **9**, 37–46.
112 P. Adhav, D. Pawar, B. Diwate, M. Bora, S. Jagtap, A. Chourasia, S. Dallavalle and V. Chabukswar, *Synth. Met.*, 2023, **293**, 117237.
113 Sh. Nasresfahani, Z. Zargarpour, M. H. Sheikhi and S. F. Nami Ana, *Synth. Met.*, 2020, **265**, 116404.
114 G. Chen, Y. Yuan, M. Lang, Z. Lv, W. Ma, N. Gu, H. Liu, J. Fang, H. Zhang and Y. Cheng, *Appl. Surf. Sci.*, 2022, **598**, 153821.
115 R. K. Pippara, P. S. Chauhan, A. Yadav, V. Kishnani and A. Gupta, *Microsyst. Nanoeng.*, 2021, **12**, 100086.
116 J.-H. Lee, J.-Y. Kim, M.-S. Nam, A. Mirzaei, H. W. Kim and S. S. Kim, *Sens. Actuators B Chem.*, 2023, **375**, 132868.
117 J.-H. Lee, J.-Y. Kim, A. Mirzaei, M.-S. Nam, H. W. Kim and S. S. Kim, *Sens. Actuators B Chem.*, 2023, **374**, 132850.
118 X. Xing, L. Du, D. Feng, C. Wang, Y. Tian, Z. Li, H. Liu and D. Yang, *Sens. Actuators B Chem.*, 2022, **351**, 130944.
119 R. Pal, S. L. Goyal and I. Rawal, *Iran. Polym. J.*, 2022, **31**, 519–532.
120 S. K. Singh, R. K. Shukla, R. Kumar, U. K. Tripathi and S. K. Mishra, *Mater. Lett.*, 2022, **309**, 131325.
121 S. Kafash and H. Milani Moghaddam, *Int. J. Hydrog. Energy*, 2022, **47**, 14740–14758.
122 Q. Hu, Z. Wang, J. Chang, P. Wan, J. Huang and L. Feng, *Sens. Actuators B Chem.*, 2021, **344**, 130179.
123 F. Ahmadi Tabar, A. Nikfarjam, N. Tavakoli, J. Nasrollah Gavgani, M. Mahyari and S. G. Hosseini, *Microchim. Acta*, 2020, **187**, 293.
124 R. Bahru, M. F. M. A. Zamri, A. H. Shamsuddin and M. A. Mohamed, *J. Mater. Sci.: Mater. Electron.*, 2020, **31**, 1574–1584.

125 L.-H. Xu and T.-M. Wu, *J. Mater. Sci.: Mater. Electron.*, 2020, **31**, 7276–7283.
126 Y. Zhang, J. Zhang, Y. Jiang, Z. Duan, B. Liu, Q. Zhao, S. Wang, Z. Yuan and H. Tai, *Sens. Actuators B Chem.*, 2020, **319**, 128293.
127 N. Belkhamssa, M. Ksibi, A. Shih and R. Izquierdo, *IEEE Sens. J.*, 2021, **21**, 9716–9722.
128 S. B. Kulkarni, Y. H. Navale, S. T. Navale, F. J. Stadler, N. S. Ramgir and V. B. Patil, *Sens. Actuators B Chem.*, 2019, **288**, 279–288.
129 G. Fan, D. Chen, T. Li, S. Yi, H. Ji, Y. Wang, Z. Zhang, G. Shao, B. Fan, H. Wang, H. Xu, H. Lu, Y. Zhou, R. Zhang and J. Sun, *Sens. Actuators B Chem.*, 2020, **312**, 127892.
130 C. Liu, H. Tai, P. Zhang, Z. Yuan, X. Du, G. Xie and Y. Jiang, *Sens. Actuators B Chem.*, 2018, **261**, 587–597.
131 C. Wang, Y. Cai, W. Zhou, P. Chen, L. Xu, T. Han, Y. Hu, X. Xu, B. Liu and X. Yu, *ACS Appl. Mater. Interfaces*, 2022, **14**, 12630–12639.
132 Q. Feng, H. Zhang, Y. Shi, X. Yu and G. Lan, *Polymers*, 2021, **13**, 1360.
133 C. Aranthady, G. V. Shanbhag and N. G. Sundaram, *RSC Adv.*, 2022, **12**, 15759–15766.
134 S. K. Gautam, N. A. Gokhale and S. Panda, *Flex. Print. Electron.*, 2022, **7**, 035022.
135 H. Xu, J. Li, P. Li, J. Shi, X. Gao and W. Luo, *ACS Appl. Mater. Interfaces*, 2021, **13**, 49194–49205.
136 A. Liu, S. Lv, L. Zhao, F. Liu, J. Wang, R. You, Z. Yang, J. He, L. Jiang, C. Wang, X. Yan, P. Sun and G. Lu, *Sens. Actuators B Chem.*, 2021, **330**, 129313.
137 K. K. Saravanan, P. Siva Karthik, P. R. Mirtha, J. Balaji and B. Rajeshkanna, *J. Mater. Sci.: Mater. Electron.*, 2020, **31**, 8825–8836.
138 H. M. Aliha, A. A. Khodadadi, Y. Mortazavi and M. N. Lotfollahi, *Appl. Surf. Sci.*, 2023, **615**, 156381.
139 Q.-Y. Zheng, M. Yang, X. Dong, X.-F. Zhang, X.-L. Cheng, L.-H. Huo, Z. Major and Y.-M. Xu, *Rare Met.*, 2023, **42**, 536–544.
140 M. Bonyani, S. M. Zebarjad, K. Janghorban, J.-Y. Kim, H. W. Kim and S. S. Kim, *Chemosensors*, 2022, **10**, 388.
141 T. Murugesan, R. R. Kumar, A. kumar Anbalagan, C.-H. Lee and H.-N. Lin, *ACS Appl. Nano Mater.*, 2022, **5**, 4921–4930.
142 M. Bonyani, S. M. Zebarjad, K. Janghorban, J.-Y. Kim, H. W. Kim and S. S. Kim, *Ceram. Int.*, 2023, **49**, 1238–1249.
143 C. Wang, H.-Y. Yu, Z. Miao, D. Ge, S. Y. H. Abdalkarim and J. Yao, *ACS Sustain. Chem. Eng.*, 2022, **10**, 6573–6583.
144 Z. M. Ali, M. N. Murshed, M. E. El Sayed, A. Samir, R. M. Alsharabi and M. O. Farea, *Opt. Mater.*, 2023, **144**, 114324.
145 H. Chen, Y. Chen, H. Zhang, D. W. Zhang, P. Zhou and J. Huang, *Adv. Funct. Mater.*, 2018, **28**, 1801035.
146 A. Liu, S. Lv, L. Jiang, F. Liu, L. Zhao, J. Wang, X. Hu, Z. Yang, J. He, C. Wang, X. Yan, P. Sun, K. Shimanoe and G. Lu, *Sens. Actuators B Chem.*, 2021, **332**, 129444.
147 G. Liu, Y. Zhou, X. Zhu, Y. Wang, H. Ren, Y. Wang, C. Gao and Y. Guo, *Sens. Actuators B Chem.*, 2020, **323**, 128699.
148 A. Akbar, M. Das and D. Sarkar, *Sens. Actuator A Phys.*, 2020, **310**, 112071.
149 N. Li, Y. Jiang, C. Zhou, Y. Xiao, B. Meng, Z. Wang, D. Huang, C. Xing and Z. Peng, *ACS Appl. Mater. Interfaces*, 2019, **11**, 38116–38125.
150 D. Xiong, X. Li, Z. Bai and S. Lu, *Small*, 2018, **14**, 1703419.
151 H.-F. Zhang, J.-Y. Xuan, Q. Zhang, M.-L. Sun, F.-C. Jia, X.-M. Wang, G.-C. Yin and S.-Y. Lu, *Rare Met.*, 2022, **41**, 3976–3999.
152 H. Zhi, X. Zhang, F. Wang, P. Wan and L. Feng, *ACS Appl. Mater. Interfaces*, 2021, **13**, 45987–45994.
153 Y. Cai, Y. Wang, X. Wen, J. Xiong, H. Song, Z. Li, D. Zu, Y. Shen and C. Li, *Anal. Chim. Acta*, 2022, **1225**, 340256.
154 X. Li, J. Xu, Y. Jiang, Z. He, B. Liu, H. Xie, H. Li, Z. Li, Y. Wang and H. Tai, *Sens. Actuators B Chem.*, 2020, **316**, 128144.
155 X. Wen, Y. Cai, X. Nie, J. Xiong, Y. Wang, H. Song, Z. Li, Y. Shen and C. Li, *Sens. Actuators B Chem.*, 2023, **374**, 132788.
156 S. Wang, B. Liu, Z. Duan, Q. Zhao, Y. Zhang, G. Xie, Y. Jiang, S. Li and H. Tai, *Sens. Actuators B Chem.*, 2021, **327**, 128923.
157 S. Wang, Y. Jiang, B. Liu, Z. Duan, H. Pan, Z. Yuan, G. Xie, J. Wang, Z. Fang and H. Tai, *Sens. Actuators B Chem.*, 2021, **343**, 130069.
158 S. Yang, V. V. Karve, A. Justin, I. Kochetygov, J. Espín, M. Asgari, O. Trukhina, D. T. Sun, L. Peng and W. L. Queen, *Coord. Chem. Rev.*, 2021, **427**, 213525.
159 G. Mashao, K. D. Modibane, S. B. Mdluli, E. I. Iwuoha, M. J. Hato, K. Makgopa and K. M. Molapo, *Electrocatalysis*, 2019, **10**, 406–419.
160 J. Lin, G. Li, C. She, Y. Zhang, S. Liu, C. Jing, Y. Cheng and J. Chu, *Mater. Res. Bull.*, 2022, **150**, 111770.
161 D. Zhang, Z. Kang, X. Liu, J. Guo and Y. Yang, *Sens. Actuators B Chem.*, 2022, **357**, 131419.

